University of Tennessee, Knoxville

TRACE: Tennessee Research and Creative Exchange

Doctoral Dissertations

Graduate School

5-2017

Experiment and simulation of single-molecule recycling

Bo Wang
University of Tennessee, Knoxville, bwang14@vols.utk.edu

Follow this and additional works at: https://trace.tennessee.edu/utk_graddiss

Part of the Atomic, Molecular and Optical Physics Commons

Recommended Citation

Wang, Bo, "Experiment and simulation of single-molecule recycling. " PhD diss., University of Tennessee, 2017.
https://trace.tennessee.edu/utk_graddiss/4436

This Dissertation is brought to you for free and open access by the Graduate School at TRACE: Tennessee Research and Creative Exchange. It has been accepted for inclusion in Doctoral Dissertations by an authorized administrator of TRACE: Tennessee Research and Creative Exchange. For more information, please contact trace@utk.edu.

To the Graduate Council:

I am submitting herewith a dissertation written by Bo Wang entitled "Experiment and simulation of single-molecule recycling." I have examined the final electronic copy of this dissertation for form and content and recommend that it be accepted in partial fulfillment of the requirements for the degree of Doctor of Philosophy, with a major in Physics.

Lloyd M. Davis, Major Professor

We have read this dissertation and recommend its acceptance:

Marianne Breinig, Chris Parigger, Feng-Yuan Zhang, Horace W. Crater

Accepted for the Council:

Dixie L. Thompson

Vice Provost and Dean of the Graduate School

(Original signatures are on file with official student records.)

Experiment and simulation of single-molecule recycling

A Dissertation Presented for the
Doctor of Philosophy
Degree
The University of Tennessee, Knoxville

Bo Wang
May 2017

ACKNOWLEDGEMENTS

I dedicate this dissertation to my parents, without whose love and support over the years it would not have been possible for me to follow my dreams. I am grateful for financial support for my research from the Center for Laser Applications, the University of Tennessee Space Institute, and the National Science Foundation grant No. 100408. I would like to thank my committee, Profs. Feng-Yuan Zhang, Chris Parigger, and Marianne Breinig: Without their help, I would not have conquered the difficulties in my studies to complete my dissertation. Finally, I would like to thank Prof. Lloyd Davis and Dr. Brian Canfield: They gave me the best assistance in my research and taught me better ways to solve problems.

ABSTRACT

This dissertation presents theoretical, numerical, and experimental research into a technique for extending the observation time of a single molecule in solution, while also enabling measurement of its diffusion coefficient. A confocal microscope is used to observe the fluorescently labelled molecule in aqueous solution, which is confined within a nanochannel. By focusing a laser beam into the nanochannel and applying electrokinetic flow along the tube, a molecule passes through the laser beam and emits a burst of photons. The molecule then passes back and forth through the focus while the voltage is repeatedly reversed at a fixed delay after each detected burst. First, a Monte Carlo simulation of the single-molecule recycling (SMR) process is made to develop algorithms for timing the flow reversals and to study the choice of experimental parameters for diffusivity measurements. To detect fluorescence bursts from the background, a weighted sliding sum algorithm is applied, and the results show it has clear advantages over a previously used photon binning algorithm. Maximum-likelihood methods are developed to measure single-molecule diffusivities and their confidence limits from the variation in the times between detections. The simulations show that SMR can distinguish single molecules with diffusivities differing by a factor of ~1.3 or less, which is smaller than that resolvable in ensemble experiments by fluorescence correlation spectroscopy. Simulations are also developed to study both 1 and 2-photon excitation of ultrasmall CdSe quantum dots, which exhibit fluorescence intermittency or blinking. The simulation incorporates standard photophysics in such a way as to account for the known non-ergodic power-law

dependence of the blinking intervals. For SMR experiments, two configurations are implemented: capillary microchannel devices are fabricated and used with a piezo system to provide motion, and nanochannels from a previous research project are used with applied voltage to give electroosmotic motion. A real-time control system that implements the weighted sliding sum and motion switching algorithms studied in the simulations is developed. The results from the experiments demonstrate SMR for 40 nm fluorescently labelled beads for hundreds of times and yield diffusion coefficients in the magnitude of 10^{-13} m^2s^{-1} in a nanochannel.

TABLE OF CONTENTS

CHAPTER 1: INTRODUCTION 1
CHAPTER 2: NUMERICAL MODELING AND ANALYSIS 7
2.1 Components of the simulation 7
2.2 Matched filter for photon burst detection 10
2.3 Determining the time of passage and reversing the flow 12
2.4 Maximum-likelihood estimation of single-molecule diffusivity 20
CHAPTER 3: SIMULATION RESULTS FOR SINGLE-MOLECULE RECYCLING . 33
3.1 Simulation of single-molecule recycling 33
3.2 Measuring diffusivities and resolving different species 42
CHAPTER 4: SIMULATION FOR A QUANTUM DOT AND TWO-PHOTON EXCITATION EXPERIMENT 45
4.1 Energy levels of quantum dots 45
4.2 Simulation of photokinetics for a single quantum dot 49
4.3 Two-photon excitation experiment 57
CHAPTER 5: EXPERIMENTAL APPARATUS 62
5.1 Laser systems and fluorescence collection 62
5.2 Real-time control system 66
5.3 Microfluidic devices 72
CHAPTER 6: EXPERIMENTAL RESULTS 81
6.1 Measurement of beam waist and velocity 81
6.2 Results from single-molecule recycling in a capillary microchannel 85
6.3 Results from single-molecule recycling in a nanochannel 92
CHAPTER 7: SUMMARY AND FUTURE WORK 96
LIST OF REFERENCES 98
APPENDIX 103
VITA 105

LIST OF TABLES

Table 1: Parameters used in MC simulations. 34
Table 2: Parameters used in the 1PE simulation..... 50

LIST OF FIGURES

Fig. 1: Statistics of fluctuations in peak values of the WSS from which the threshold is determined (see text for details). 13
Fig. 2: Comparison of timing errors found by four different methods (see text for details). 16
Fig. 3: Algorithm for single-molecule recycling. 18
Fig. 4: Probability density function of interval between molecule passages, as given by Eq. (2-11). 24
Fig. 5: The pdf of *D* in non-dimensionalized units, from which the ML estimate of *D* and its confidence limits are determined. 27
Fig. 6: Evolution of the probability density function of diffusivity *D* as a single molecule is recycled up to 200 times. 32
Fig. 7: Histograms of times between passages. 36
Fig. 8: Example of the trajectory of a molecule as it transits the laser focus. 38
Fig. 9: Trajectories of a molecule undergoing SMR, with parameters from Table 1. 40
Fig. 10: Plot of ML estimated diffusivities versus numbers of recycles. 43
Fig. 11: DNA 13mers and DNA 15mers are resolved by estimating their diffusivities. The two vertical lines are diffusivities of the two species [23]. 44
Fig. 12: The diagram of the energy levels of a QD and the transitions between them. 47
Fig. 13: The photon counts from a single immobilized QD by a simulation of 1PE. 51
Fig. 14: Comparison of histograms of "on" periods obtained from (A) simulations, and (B) an experiment, as reported in Fig. 7 of Ref. [40]. 53
Fig. 15: Occurrences of (A) "on" periods and (B) "off" periods for constant trapping and detrapping lifetimes. Occurrences of (C) "on" periods and (B) "off" periods for variable trapping and detrapping rates. 54
Fig. 16: (A) Photon counts of single QD by a simulation of 2PE. (B) Occurrences of "on" periods. (C) Occurrences of "off" periods. 56

Fig. 17: (A) Histogram of a single QD's number of recycles before it leaves recycling. (B) Histogram of times between detections. The minor peaks represent misdetections..... 58
Fig. 18: (A) Laser system for 2PE. (B) Zemax design of beam expander for the femtosecond laser beam (The lenses are Newport KPC019, KBX061, KPC031.) Inset shows the focus is close to diffraction limited. 59
Fig. 19: (A) Photon bursts from single molecules of Rhodamine B, (B) FCS from the two SPADs..... 61
Fig. 20: A schematic of the experimental apparatus for SMR..... 63
Fig. 21: (A) Configuration of the beam expander and the microscope. (B) Beam sampler, EM-CCD, pinhole, and SPADs. 65
Fig. 22: Zemax design of beam expander to collimate the beam and fill the objective pupil (A) The three lenses are Newport KPC019, KBX064, KPC031, (B) The three lenses are Newport KPC031, KBX064, KPC019)..... 67
Fig. 23: Control flow of the LabView real-time program. 69
Fig. 24: (A) The block diagram for WSS on the target PC. (B) The block diagram for voltage control on the FPGA. 71
Fig. 25: (A) A nanochannel device is mounted on the confocal microscope, the syringes connect to two microchannels. (B) The housing of the nanochannel device. (C) The contour of the microchannels, which are linked by ten nanochannels. (D) The laser beam focuses into one of the nanochannels. When a molecule goes through the laser spot, the fluorescence is collected by the objective. 73
Fig. 26: SMR of 40 nm Fluospheres® in 50% methanol aqueous solution. The reversal delay is 10 ms. The WSS peaks show the molecule can be recycled, but the sticking still appears to be present. 74
Fig. 27: SMR with a solution of 1 nM 40 nm Fluospheres, 1×TAE buffer, and 0.02% Tween-20. The reversal delay is 30 ms. 76

Fig. 28: (A) ACFs of dsDNA molecules driven by different voltages. (B) Result from an attempt at SMR using labeled dsDNA. 77

Fig. 29: (A) The size of the capillary tubing. (B) A finished capillary microchannel device. The o-rings on the sides are reservoirs of solution, and the o-ring in the middle is the observation window for the objective. This o-ring is filled with immersion oil to reduce refraction and reflection from the outer wall of the capillary. Two electrodes are connected to the reservoirs by platinum wires. (C) SMR using the piezo of a Fluosphere that appears to be freely diffusing along the capillary. The reversal delay is 30 ms. 79

Fig. 30: (A) ACF of Alexa 647 conjugates free diffusing on a coverslip. ω_0 is measured by fitting the function. (B) ACF of Fluospheres recycling in a nanochannel. v is measured from ω_0 and the fitted curve. 82

Fig. 31: Fit of the data in Fig. 29 (A) to Eq. (6-1). 84

Fig. 32: ACF of immobilized Fluospheres in SMR using the laser beam for the capillary microchannel. 86

Fig. 33 (A) Blue solid line is the trajectory of the piezo stage, the red dot is the center of the recycling. (B) The red dot is $t_w(i) - t_p(i)$ in each recycle. (C) The algorithm applied in the SMR with the piezo stage. 88

Fig. 34: Histograms of the gap between the peaks and the starts. The center of the effective distributions are (A) 2.516 ms, (B) 2.575 ms, (C) 2.575 ms, (D) 2.63 ms. 90

Fig. 35: Results from SMR in the capillary microschannel with the piezo stage. The upper graph shows the variations of centers of recyles. The bottom graph illustrates the estimated diffusivities of individual Fluospheres, which forms a Gaussian distribution centered around 1.8×10^{-10} m^2s^{-1}. 91

Fig. 36: The histograms of times between concecutive detections. (A) The center of the distribution is 60 ms. (B) Two distributions overlaps. The center of the left peak is 39.85 ms, and the center of the right peak is 40.14 ms. (C) The center of the distribution is 40 ms. 93

Fig. 37: The fitted histogram of Fig. 37 B. 94
Fig. 38: The estimated diffusivities of 40 nm Fluospheres..... 95

CHAPTER 1: INTRODUCTION

Fluorescence detection of individual molecules in solution provides the basis for a number of useful capabilities, for example, observation of molecular heterogeneities and dynamical processes that cannot be synchronized between members of an ensemble [1]. Compared to wide-field imaging, confocal fluorescence microscopy offers superior signal-to-noise, because the excitation laser beam is tightly focused and fluorescence is collected only from the small confocal volume [2]. It also enables faster time resolution, because instead of the fluorescence being imaged with a camera, it is focused to a point detector, such as a single-photon avalanche diode (SPAD), which can measure the timing of each detected photon to sub-nanosecond precision. On the other hand, for a single molecule in solution, Brownian diffusion limits the time that the molecule remains in the confocal volume to a millisecond or less. Extending the observation time is important for improving the precision of spectroscopic measurements and for witnessing dynamical changes. However, prolonged observation by immobilizing a molecule to a surface alters its local environment and may stereo-chemically restrict interactions [3, 4]. Likewise, laser tweezers can be used to hold particles and biomolecules of size down to ~100 nm, or ~10 nm in the case of near-field traps, but the required laser trap intensities usually give perturbations due to heating, resulting for example in protein unfolding [5].

Feedback-driven tracking and trapping, in which repeated measurement of the displacement of the molecule from the center of the confocal volume is used for real-time control of the sample position or focused laser position, offers extended observation time

with potentially less perturbation than optical trapping [6]. Enderlein first proposed feedback-driven tracking using a confocal microscope [7]. He used a rotating laser spot position to determine the SM position and a feedback-driven piezo positioning system to counteract the Brownian motion and enable longtime observation of a SM diffusing in two dimensions (2-D). Subsequently, Cohen and Moerner developed a 2-D anti-Brownian electrokinetic (ABEL) trapping method to achieve prolonged observation of fluorophores and labeled proteins in liquid environments [6, 8-10]. In research at UTSI, electrokinetic trapping of a fluorescently-labeled protein in a nanochannel (a 1-D ABEL trap) [11, 12], 3D electrokinetic trapping of a 40 nm fluorescently-labeled nanoparticle in solution [13], and 3D feedback-driven tracking of a 20 nm fluorescent nanoparticle in solution with a piezo stage [14] have been developed. However, the feedback for such methods, with either piezo [14-16] or electrokinetic [17] repositioning in one [11], two [8, 10], or three [13, 18] dimensions, requires a continuous fluorescence signal and thus sustained excitation, and hence the observation duration of the molecule may be limited by photobleaching and/or photoblinking caused by crossing to a triplet or dark state.

Single-molecule recycling (SMR) in a nanochannel, in which the molecule quickly passes through the laser beam and the solution flow is reversed after a set delay following each passage, is an alternative to feedback-driven trapping that offers new possibilities for single-molecule measurements [19]. As the molecule passes through the area of laser radiation periodically, there is opportunity for recovery from photogenerated reversible dark states and the time before irreversible photobleaching is highly extended. Even if

some passages are not detected, the flow may be reversed following each anticipated passage and thus the overall observation duration can be prolonged to more than 10 s [19]. In other nanochannel-based single-molecule fluorescence research, Craighead et al. introduced a method for single-molecule analysis of epigenetic states of DNA by driving electrokinetic flow in a nanochannel [20, 21]. Ghosh et al. made PDMS nanochannels on fused silica substrate, aiming to implement ABEL trap in the nanochannels [22].

In Chapter 2, we present Monte Carlo (MC) simulations and we apply parameters from previously published works [19, 23] to model the process of SMR. We use improved methods to ascertain the projected capability of burst detection and to developed algorithms for SMR in my experiments. The approach is similar to that in the first report on photon burst detection of a single-chromophore molecule in solution [24], where MC simulations were used to validate experimental results and determine feasibility limits for future experiments, and where a digital filter was used to enhance photon bursts for clearer discrimination from background. Although this and other early MC simulations of single-molecule detection used course-grained algorithms to model the number of detected photons in sequential time intervals [25, 26], an algorithm for simulating the time-of-arrival of each detected photon was subsequently developed by use of variable time intervals for the different physical processes, and it was used it to study fluorescence correlation spectroscopy (FCS) [27] and feedback-driven trapping in a nanochannel [23]. The MC simulation in this dissertation uses this same fine-grained algorithm to model the physical and instrumental processes and generate the time of each photon, while for burst detection

with improved timing and discrimination from background, it employs maximum-likelihood (ML) analysis of the photon times and a matched digital filter [28], i.e., a filter with a Gaussian impulse response equal to the expected fluorescence profile from a molecule passing at constant speed through the laser focus. To model SMR, the simulation includes an algorithm for flow reversal a set time delay *T* after each detected or anticipated passage with provision for reloading with a new molecule following photobleaching or interruption of the SMR by an "invader" molecule.

In addition to prolonged observation times, SMR provides a means for experimentally investigating molecular motion, interactions, and transport in nano-confined spaces, topics of increasing interest [29]. To this end, we apply MC simulations to investigate capabilities for SMR measurements of the diffusivity of a single molecule in a nanochannel. The diffusivity may be determined from the fluctuations in the intervals between detected photon bursts, hence the need for precisely determining the times of the photon bursts by use of the matched filter and ML analysis. In fluidic systems, the diffusivity of a molecule depends on its size and shape and the properties of the suspending medium, making it an important nanoscale characteristic. Diffusivity in a nanochannel may differ from that in bulk solution [30, 31]. In pharmaceutical drug discovery research, molecular interactions can be probed by the slow-down in the diffusivity of fluorescent ligands when they become bound to larger biomolecules [27]. For such studies, the mean diffusivity of an ensemble of molecules in solution may be measured by FCS [32, 33] or 2-focus FCS [34] by fitting the autocorrelation function. Mixtures of molecules with different diffusivities can be

resolved by FCS, but species with diffusivities differing by less than a factor of about 1.6 are not resolvable [35]. In contrast to such ensemble measurements, the diffusivity of a single molecule can be determined in feedback-driven tracking and trapping experiments by fitting the mean-square displacement of the molecule's trajectory, while accounting for corrective motions of the feedback system [36, 37]. In tracking experiments, the precision of the measured diffusion coefficient depends much more on the duration of the trajectory or number of frames than on the information content of each frame [38].

SMR provides an alternate method for single-molecule diffusivity measurements that is applicable to the confines of a nanochannel. In this dissertation, we develop a ML strategy for measuring single-molecule diffusivity, which is valid even for a small number of detected photon bursts. In doing so, we restrict possible diffusivity values to a finite range $0 < D < D_{\max}$, where $D_{\max}$ depends on the time delay T between molecule passage and flow reversal, which limits the maximum measurable fluctuation in the interval between detected photon bursts due to diffusion. The likelihood function may be normalized over the finite domain to give the probability density function (pdf) for the diffusivity estimate, which also enables determining the confidence limit or statistical error of the estimate. In Chapter 3, we determine experimental parameters that increase the number of recycles and use MC simulations to show that by collecting the timings from a sufficient number of photon bursts (~200), it should be possible to resolve single molecules with diffusivities that differ by a factor of 1.3, i.e., a smaller amount than is practically resolvable by FCS. In Chapter 4, we develop simulations of fluorescence from immobilized quantum dots

(QDs) based on an Auger ionization model [39] and we compare the results with the experimental outcomes of others [40]. We also present simulations of SMR of QDs with two-photon excitation (2PE) and some experimental results of 2PE of rhodamine B. In Chapter 5, we present details on the experimental apparatus and the preparation of the microfluidic devices. In Chapter 6, we describe the data analysis techniques and experimental results. The experiments include SMR of 40 nm Fluospheres® (fluorescently labelled latex beads), which can be recycled for more than one thousand times, and which are found to have diffusion coefficients in the nanochannel of about 10^{-13} m^2s^{-1}.

CHAPTER 2: NUMERICAL MODELING AND ANALYSIS

The purpose of this chapter is to introduce a theoretical model of the photophysical processes and motion of molecules in a nanochannel, in terms of which we numerically model SMR and analytically describe the statistical features needed for SMR measurements. We thereby develop a method for ML estimation of the diffusivity of the molecule.

2.1 Components of the simulation

As mentioned in the introduction, the Monte Carlo simulation algorithms used in this dissertation are based on those described by Robinson et al. for single-molecule trapping in a nanochannel [23], but the simulation program is completely rewritten and incorporates additional algorithms for flow reversal. The code is written in C++ and compiled using the Intel compiler. The main components are briefly reviewed below.

Molecules move by electrokinetic flow and diffusion along a finite 1-dimensional (1D) grid, which represents the length of the nanochannel. For accurate modeling, the grid spacing, which is typically taken to be Δx = 10 nm, must be much smaller than the waist of the focused laser beam. To model flow (and electrophoretic motion) at a velocity v, all molecules move 1 grid space in the direction of the flow at fixed intervals of $\Delta t_F = \Delta x/v$. At each of these times, there is a probability $p_F = 10^3\, N_A\, A\, \Delta x\, C$ that a new molecule may enter the upstream end of the grid, where N_A is Avogadro's number, A is the cross-sectional area of the nanochannel in m^2, and C is the molar concentration of molecules in the

upstream reservoir; hence with the entry of each new molecule, a geometrically distributed random unsigned integer with mean $1/p_F$ is generated to determine the number of flow intervals until the next such molecule. To efficiently model diffusion with diffusivity D, molecules on the grid hop to random nearby places at fixed intervals of $\Delta t_D = \Delta x^2/(2D)$. At each of these times, for each molecule a uniform random unsigned integer (U32) is compared to a look-up table of 13 values to determine the number of spaces to hop (Gaussian distributed between –6 and 6, with mean of 0 and standard deviation 1, with look-up values obtained from Table 1 of [23]). At each of these times, there is a probability p_D that a new molecule may enter by diffusion onto a random place near either end of the grid; hence the number of diffusion intervals until the next such new molecule is a geometrically distributed random unsigned integer with mean $1/p_D$. When a molecule enters, its initial random place near either end is determined by comparing a uniform random number (U32) with values in a look up table (obtained from Table 2 of [23] and found by summing the probabilities for all possible ways of entry), while p_D is similarly determined by summing all possibilities and found to be $p_D = 0.76\ p_F$ (eqn. (15) of [23]). An "invader" molecule could enter the nanochannel while another is being recycled. To reduce the possibility that SMR is disrupted by an invader, we can lower the concentration C in the reservoirs and thereby reduce the chance of a new molecule entering. Invader molecules may also be distinguished by the recycling algorithm, as discussed below in section 2.3.

In addition to motion of molecules on the grid, the MC simulation must also follow the photophysical processes of each molecule, including excitation, triplet crossing, photobleaching, and relaxation processes, with or without photon detection. Also, instrumental effects including detector dead time, afterpulses, and background counts are simulated. These many possible processes occur in sequence in an interdependent manner. To model them and generate the time-of-arrival of each photon detected by the SPAD, the simulation uses calls to random numbers with appropriate continuous or discrete distributions to find the possible times of the next occurrences for all possible processes, for the given initial conditions. For example, when a molecule returns to the ground state, an exponentially distributed random number with mean equal to the reciprocal of the excitation rate at the present location is used to determine when the molecule would transition to the excited state for continuous laser excitation (unless it were to move before this time), whereas for pulsed excitation, a geometrically distributed random number with mean equal to the reciprocal of the probability for excitation per laser pulse is used to determine the number of pulses before the next excitation. The various processes considered include the next (1) flow time-step, (2) diffusion time-step, (3) photophysical event for any of the molecules in the simulation, (4) detection of a background photon, (5) detection of a fluorescence photon, and (6) resetting of the flow direction to effect recycling. The simulation then determines the process with the minimum time (using the idamin() function of the Math Kernal Library of the Intel compiler), advances to that time, and then re-evaluates the next possible times for all possible processes with the new initial

conditions. With each advance in time, the stream of photon detection times is processed to search for photon bursts and possibly reschedule the next change in flow direction.

2.2 Matched filter for photon burst detection

To detect the passage times of molecules through the laser focus, photon bursts must be recognized above the background. In previously published SMR experiments [19], photons were counted into successive 1 ms bins using a PCI-6602 counter card and LabVIEW (National Instruments), and two different thresholds were used to distinguish signal from background noise. A molecule passage was detected if successive bins each had 7 or more photons and if there were at least 40 photons in total (supplemental information of [19]). However, the 1 ms binning limits the precision of the estimated time of passage. In addition, the authors note that the time resolution of their feedback was limited by a 2 ms LabVIEW loop time, and that faster time resolution could be possible by analyzing photon arrival times with use of a FPGA or LabVIEW RealTime system.

Therefore, in order to improve the timing of bursts and their discrimination from background, the simulation investigates time-stamping each photon and processing the stream of photon times by a weighted sliding sum (WSS), in which the weights are proportional to the expected temporal profile of the fluorescence signal as a molecule passes through the laser focus. Thus the WSS ideally corresponds to a matched digital filter [19]. For a molecule passing at constant velocity v through a Gaussian laser focus of waist ω_0, the weights are taken to be $w(t) \propto \exp(-(t-3\sigma_t)^2/(2\sigma_t^2))$, $0 \le t \le 6\sigma_t$, where the width of the weight function is ideally $\sigma_t = \omega_0/(2v)$. On the other hand, the WSS can be successfully

implemented with Gaussian weights even if the width is non-ideal, as may occur if the experimental value of $\omega_0/(2v)$ is not accurately measured, if the experiment is using different types of molecules with differing electrophoretic velocities v, or if diffusion causes the effective transit velocity through the laser focus to fluctuate. In most results presented below, we set σ_t = 1.5 ms, whereas the ideal width is $\omega_0/(2v)$ = 1.41 ms. We will explain how the ratio $\omega_0/(2v)$ can be experimentally measured by fitting the normalized autocorrelation function calculated from the photon times in Chapter 4.

To efficiently implement the digital filter, the weights at discrete intervals of Δt_W = 10 μs are stored in an array [`for(i=0;i<sig6;i++) w[i]=(unsigned short int)(a*exp((i-b)^2/c);` where `a=128.0,` `b=3`σ_t /Δt_W, , `c=2(`σ_t /Δt_W`)^2`, `sig6=6`σ_t /Δt_W] and whenever a photon is detected, these values are added to another array of equal length [`for(i=0;i<sig6;i++) s[i]+=w[i];`]. Then, at intervals of Δt_W = 10 μs, the WSS is simply read from the first element of this array and the array is displaced [`WSS=s[0]; for(i=0;i<sig6-1;i++) s[i]=s[i+1]; s[sig6-1]=0;`]. The value `a=128.0` is chosen to give suitable dynamic range with fast unsigned short integer calculations. We have found that the WSS can be computed in real time in this way in a LabVIEW Realtime program with NI-PCI-7833R FPGA data acquisition card. The portion of the LabVIEW code for doing this is shown in Chapter 5.

As time progresses and the WSS is updated, all successive peaks and valleys are found, while ignoring fluctuations that are < ±64 (`a/2`). To distinguish photon bursts due to the passage of a molecule from those due to background, peaks in the WSS must be above a

preset threshold, as seen in Fig. 1. The threshold may be chosen by recording the statistics of background-induced fluctuations in the WSS while no molecules pass, as seen in the insets of Fig. 1. The main plot shows a histogram of peak values of the WSS during a 10^4 s simulated experiment. The solid red line is a threshold at an amplitude of 1750, also indicated by the red cross in the upper inset and found by the point of intersection of the red dashed line with the x-axis in the lower inset. The upper inset shows a plot of the thresholds at which there is a false peak rate of 1 per 10^2 s versus the background count rate for WSS weights of widths σ_t = 1.0 ms, 1.5 ms, and 2.0 ms. The lower inset shows the number of peaks below threshold versus threshold during 10^4 s simulations with σ_t = 1.5 ms and background rates of 400, 600, and 800 s^{-1}. Similar curves are used to generate the data in the upper inset. In principle, peaks due to background can be further discriminated by only retaining those that occur within preset limits of the expected time of passage of a molecule, as explained in section 2.3. All the same, a very low rate of background peaks without such limitation is preferable for diffusivity measurements, using the ML estimation method explained in section 2.4. Hence for a background rate of 600 s^{-1}, we use a WSS threshold of 1750, which gives about 1 false peak per 10^5 s, as seen in the lower inset of Fig. 1.

2.3 Determining the time of passage and reversing the flow

Once a burst of photons from the passage of a molecule is detected, it is possible to estimate the time of passage in several ways. We use simulations of automatically recycling one molecule with no diffusion, where the exact time of passage is known, and also with

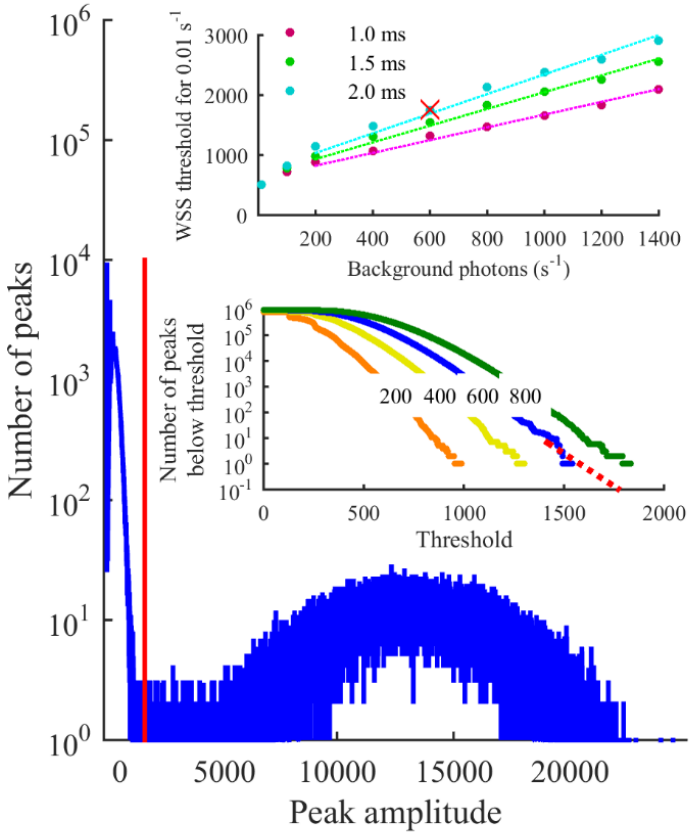

Fig. 1: Statistics of fluctuations in peak values of the WSS from which the threshold is determined (see text for details).

no photobleaching or invader molecules, to compare four different estimation methods. Method 1 is to use the algorithm of Ref. [23] and take the time at which the second threshold is reached. As expected, the precision in this case is limited by the 1 ms photon binning time. Method 2, which gives significant improvement, is to take the time of the first point at which the WSS attains its maximum value, with a correction of $-3\sigma_t$ to account for the delay between photons and the evaluation of the WSS. Method 3 is to take the midpoint of the times at the leading and trailing edges at which the WSS crosses a level that is half way between the threshold (1750) and the peak (again with $-3\sigma_t$ correction). This gives a further small improvement of about 4%, probably because photon shot noise can shift the maximum of the peak more than the edges. Method 4, which requires longer to compute, is to average the times of all photons that occur within a chosen interval around the center of the burst, which is taken to be the expected time of passage first found by method 2. In effect, this gives the ML estimate of the passage time. The derivation is as follows: The likelihood function for the time of passage t_p is

$$L\left(t_p;t_i\right)=\exp\left[-\frac{\left(t_i-t_p\right)^2}{2\sigma_t^{\,2}}\right], \tag{2-1}$$

where t_i is the detection time of the photon. The ML estimate of t_p is the value of t_p for which Eq. (2-1) is a maximum, which is found by solving $\partial L(p;t_i)/\partial p=0$, that is $\hat{t}_p=t_i$. When M independent measurements t_i are made, if each estimate is of equal reliability, the ML estimate from the set would simply be the mean of the individual measurements,

$$\hat{t}_p = \frac{1}{M}\sum_i t_i \,. \tag{2-2}$$

Results of the comparison of the different methods are summarized in Fig. 2. The main plot in Fig. 2 shows the standard deviation of the intervals between successive molecule passages as a function of laser power (with background held at 600 s^{-1}) for four methods for measuring the times of passage: M1) Collect photons in 1 ms bins and record the time at which there are successive bins with ≥7 photons and ≥40 photons in total [23]; M2) Take the time of the maximum value of the WSS peak, where the width of the Gaussian weights are σ_t = 1.5 ms; M3) Take the midpoint of the times at which the WSS crosses a threshold that is half way between the threshold (1750) and the maximum of the peak; M4) Find the ML estimate, which is the average of the detection times of photons that are within an interval of ± 3σ_t of the center of the burst, as first found by method 2. The red circles plot $\sqrt{2}\sigma_t / \sqrt{n}$, where n is the mean number of photons within the burst. The inset shows the standard deviation of the ML estimates for a laser power of 98 μW for intervals of $\pm f\sigma_t$, where f varies from 1 to 4. As shown in the inset of Fig. 2, method 4 has best precision for an interval of ±3σ_t and in this case the timing error is about 84% of that obtained by method 2. Except for method 1, the timing errors are normally distributed with standard deviations δ_t that vary with the laser power, amplitude of WSS peak, and number of photons in the burst. For the ML estimate of method 4, if n photons are detected and the expected temporal profile is a Gaussian with a standard deviation σ_t, and if background is negligible, then the estimated passage time is theoretically expected to have an error of $\sigma_t / \sqrt{n}$, and hence

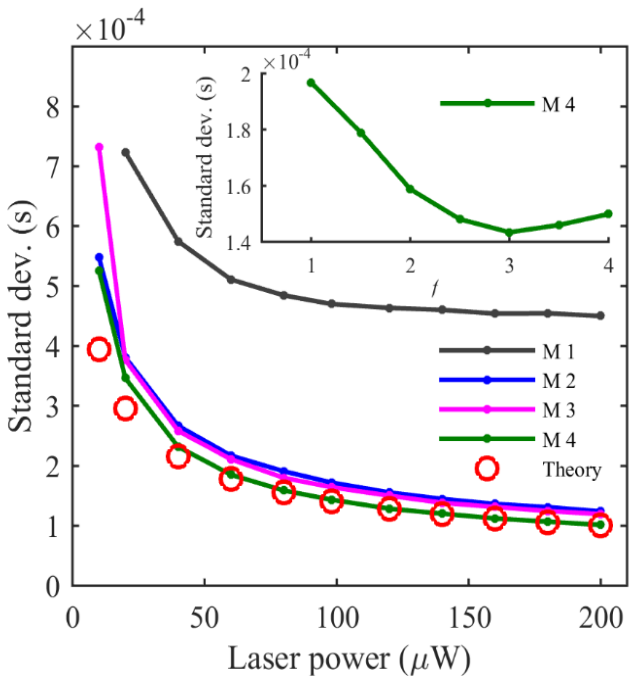

Fig. 2: Comparison of timing errors found by four different methods (see text for details).

the interval between two passages would have an error of $\delta_t = \sqrt{2}\sigma_t / \sqrt{n}$, which is shown by the red circles in Fig. 2. $\sigma_t / \sqrt{n}$, and hence the interval between two passages would have an error of $\delta_t = \sqrt{2}\sigma_t / \sqrt{n}$, which is shown by the red circles in Fig. 2.

Clearly, bursts with more photons may be more precisely timed, but on the other hand for certain SMR experiments it may be favorable to detect each passage with as few photons as possible in order to extend the number of times a molecule may be recycled before it is photobleached. Also, as seen in the inset of Fig. 2, if the interval about the center of the photon burst is increased beyond $\pm 3\sigma_t$ in order to attempt to collect more photons for the ML estimate, the precision decreases as background photons outnumber signal photons near the edges of a burst.

As soon as the passage time is estimated using one of the above four methods, it is used to decide when to schedule the next flow reversal. The algorithm for doing this has provisions for automatic recycling following missed detections, reloading a molecule following the end of recycling, e.g., due to photobleaching, and choice of terminating or continuing to recycle in the case of an invader molecule arriving out of limits. The algorithm is shown in Fig. 3.

In prior experiments [23], a single molecule can be recycled until it photobleaches, which in some cases is hundreds of times. The probability of photobleaching can be reduced by turning down the laser power, but then the signal will decrease so some passages may not be detected. Also, a molecule passage may sometimes not be detected if the molecule crosses to a dark state. Therefore, in order to automatically recycle a molecule even if its

```
Execute next possible event at time t
  Time t for photophysical event on a molecule
  …… Time t for some other possible event…

  Time t = t_R to reverse the flow:
    Is MissedDetections m ≤ M ?
    Yes: Recycle and setup next automatic recycle
         Reverse the flow direction
         Increment MissedDetections: m = m + 1
         Increment RecycleCount: r = r + 1
         Update NextExpectedPass: t_E = t_R + T
         Schedule flow reversal for t_R + 2T
    No:  Load a new molecule
         Set the flow direction to forward
         Reset RecycleCount: r = 0
         Schedule next flow reversal for time = ∞

Following each event at time t
  Bin photons or calculate WSS up to time t
    Is there a peak > threshold ?
    Yes: Find passage time t_P by method 1, 2, 3, or 4
         Determine if passage time is expected
         Is r = 0 or | t_P − t_E | < limit ?
         Yes: Replace automatic recycle
              Reset MissedDetections m = 0
              Reschedule flow reversal for t_R = t_P + T
              Update NextExpectedPass: t_E = t_P + 2T
    (a)  No: Terminate SMR if peak from an invader
              Set MissedDetections m = M + 1
              Schedule next flow reversal for t_R = t_P
              (Leads to Load a new molecule above)
or  (b)  No: Ignore unexpected peak
              Do nothing / continue
or  (c)  No: Use unexpected peak to adjust timing
             Adjust passage time to average
             Adjust t_R and t_E
```

Fig. 3: Algorithm for single-molecule recycling.

passage is not detected for up to M times in succession, whenever the time t_R has arrived to reverse the flow, if the count of missed detections m is less than or equal to M, the computer increments m and schedules the time for the next voltage switch to be a fixed delay $2T$ later, i.e., at $t_R + 2T$. On the other hand, if the count of missed detections exceeds M, then a new molecule is loaded. This is achieved by ensuring that the voltage is set so that the flow comes from the desired reservoir, resetting the count of recycles to $r = 0$, and scheduling the time for the next voltage switch to be $t_R = \infty$, so that the flow direction will be sustained until a molecule passage is detected. After loading a new molecule at the start of recycling, or during the subsequent recycling, whenever a molecule passage is detected, the computer may replace the time of the next scheduled flow reversal, following the procedure presented in the lower part of Fig. 3. Note that different actions may be taken depending on if the passage time t_P occurs at an unexpected time, as may happen, for example, if an invader molecule enters the nanochannel. For the passage to be expected, we require either that this is the first passage ($r = 0$) or that the separation between the passage time t_P and the expected passage time t_E is less than a preset limit t_L, i.e., $| t_P - t_E | < t_L$. The limit is usually taken to be $t_L = T$, since we do not expect the next passage until after the flow is reversed, but it may be taken to be $t_L = 3\sqrt{m+1}\sqrt{4D'T}/v$, if this is smaller, where D' is the anticipated diffusivity (i.e., the separation $| t_P - t_E |$ is within 3 standard deviations of the fluctuation expected from diffusion). The time of the next expected passage t_E is tracked during the recycling process by updating it to $t_P + 2T$ following each detected passage and to $t_R + T$ following each flow reversal. If a passage is

detected at a time that is out of limits, there are several possible algorithms that may be followed: (a) We could terminate the recycling and load a new molecule, as may be appropriate if the unexpected passage were due to an invader, or (b) we could simply ignore passage times that are out of limits, or (c) we could use the unexpected passage to adjust the recycling timing without switching the flow direction. The last two cases (shown at the very bottom of Fig. 3) are discussed further in Chapter 3 and are advantageous to implement when the flow does not strongly dominate diffusion, so that the molecule sometimes generates more than one burst of photons as it passes from one end of the nanochannel to the other.

Note that if in an experiment there is a time delay τ between switching the voltage and reversal of the flow, then following each voltage reversal the next would still be scheduled after a delay $2T$, but following detection of a peak at time t_P, the next voltage reversal would be rescheduled at time $t_P - 3\sigma_t + T - \tau$. (We find $\tau = 3\ \mu\text{s}$ in our experimental implementation with NI-PCI-7833R and ±10 V analog outputs to drive electrokinetic flow.) Also, if the time between flow reversals is longer than L/v, where L is the length of the nanochannel, to avoid the molecule passing out of the nanochannel and into one of the reservoirs, the voltage may be simply turned off for part of the recycle time.

2.4 Maximum-likelihood estimation of single-molecule diffusivity

The diffusivity of a single molecule in the nanochannel may be determined by using ML methods to analyze the intervals between passage times. To determine the probability

density function (pdf) of the interval, we first use the Fokker-Planck equation to describe Brownian motion and transport of flow. When a molecule in solution is confined to a nanochannel so that it is free to move in only one dimension, the Fokker-Planck equation is given by

$$\frac{\partial}{\partial t} p(x,t) = D \frac{\partial^2}{\partial x^2} p(x,t) - v \frac{\partial}{\partial x} p(x,t), \tag{2-3}$$

where $p(x,t)dx$ is the pdf to find the molecule within dx of x at time t, D is the Einstein-Stokes diffusion coefficient, and v is the flow velocity. The solution of this equation for the initial condition $p(x,t=0)dx = \delta(x)dx$ corresponding to a molecule passing to the right through the center $x=0$ of the focused laser beam at time $t=0$ is a Gaussian function with mean moving due to flow and width increasing due to diffusion:

$$p(x,t)dx = \frac{1}{\sqrt{2\pi}\sigma(t)} \exp\left[\frac{-1}{2}\left(\frac{x-\mu(t)}{\sigma(t)}\right)^2\right] dx, \tag{2-4}$$

where $\mu(t) = vt,\ \sigma(t) = \sqrt{2Dt}$. If the flow velocity is reversed at time T, the mean becomes

$$\mu(t) = v(2T - t), \quad \text{for } t > T, \tag{2-5}$$

but the width of the Gaussian continues to increase. Hence the probability that the molecule has crossed back to the left of the origin for times $t > T$ is the same as the probability that the molecule has crossed to the right of $x_0 = 2vT$ if the flow were not reversed, i.e., $P(x<0,t) = \int_{x'=-\infty}^{x'=0} p(x',t)\,dx'$, with $\mu(t) = v(2T-t)$ is the same as

$P(x > x_0, t) = \int_{x'=x_0}^{x'=\infty} p(x', t)\, dx'$, with $\mu(t) = vt$. Therefore, the pdf that the molecule crosses back to the left of the origin within dt of time t is

$$p(t)dt = \lim_{dt \to 0} \left[\frac{P(x > x_0, t + dt) - P(x > x_0, t)}{dt} \right]. \tag{2-6}$$

With the substitutions $x' = (x - \mu(t))/\sigma(t)$, $dx' = dx/\sigma(t)$, Eq. (2-4) may be expressed as $p(x,t)dx = \left(1/\sqrt{2\pi}\right)\exp\left(-x'^2/2\right) = g(x')dx'$. Hence the last term in Eq. (2-6) is $P(x > x_0, t) = \int_{x'=x_0(t)}^{x'=\infty} g(x'(t))dx' = 1 - \int_{x'=-\infty}^{x'=x_0(t)} g(x'(t))dx'$, where $x'(t) = (x - \mu(t))/\sigma(t)$, $x_0'(t) = (x_0 - \mu(t))/\sigma(t)$. So Eq. (2-6) becomes

$$p(t)dt = \lim_{dt \to 0} \left[\frac{-1}{dt} \left(\int_{-\infty}^{x_0'(t+dt)} g(x'(t+dt))dx' - \int_{-\infty}^{x_0'(t)} g(x'(t))dx' \right) \right]. \tag{2-7}$$

By the fundamental theorem of calculus, Eq. (2-7) is

$$p(t)dt = g\left(x_0'(t)\right) \frac{-dx_0'(t)}{dt} dt\,. \tag{2-8}$$

Taking the derivative of Eq. (2-8) gives

$$\frac{dx_0'(t)}{dt} = \frac{-v}{\sqrt{2Dt}} \left(\frac{1}{2} + \frac{T}{t} \right), \tag{2-9}$$

Substituting Eq. (2-9) in Eq. (2-8), we get

$$p(t)dt = \left(\frac{1}{2} + \frac{T}{t} \right) \frac{v}{\sqrt{4\pi Dt}} \exp\left\{ \frac{-v^2 (t - 2T)^2}{4Dt} \right\} dt, t \in (0, \infty), \tag{2-10}$$

which is the pdf that the molecule passes through the center of the focus $x = 0$ at time $t = 0$ and crosses back through the origin within dt of time t.

As shown in Fig. 4, this function is asymmetric with a peak at $t < 2T$, but for longer recycle times $T >> D/v^2$ it becomes well approximated by a Gaussian centered at $t = 2T$ with a width of $\sigma_D = \sqrt{4DT}/v$, i.e.,

$$p(t)dt \approx \frac{v}{\sqrt{8\pi DT}} \exp\left[\frac{-v^2(t-2T)^2}{8DT}\right] dt = g\left(t-2T, \sigma_D\right) dt, \quad t \in (0, \infty), \tag{2-11}$$

where $g(t', \sigma)$ is a Gaussian with standard deviation σ. For typical parameters, D = 10^{-10} m^2s^{-1}, v = 3.4×10^{-4} ms^{-1}, and T = 3×10^{-2} s, we have $T \approx 35D/v^2$ and $\sqrt{4DT}/v \approx 6$ ms.

In principle, the diffusivity may be estimated from just a single measurement t_i of the interval between any two molecule passages. To simplify the discussion, consider the case where the estimated passage times are exact, so the difference between two estimated passage times exactly measures the interval between two passages t_i, and there are no missed detections, so $T < t_i < 3T$. According to the ML method [41], when the measurement result t_i is inserted into Eq. (2-11), we get a function that expresses the likelihood of the parameter D for the given measurement:

$$L(D; t_i) = \left(\frac{1}{2} + \frac{T}{t_i}\right) \frac{v}{\sqrt{4\pi D t_i}} \exp\left[\frac{-v^2(t_i-2T)^2}{4Dt_i}\right], \quad D \in [0, \infty). \tag{2-12}$$

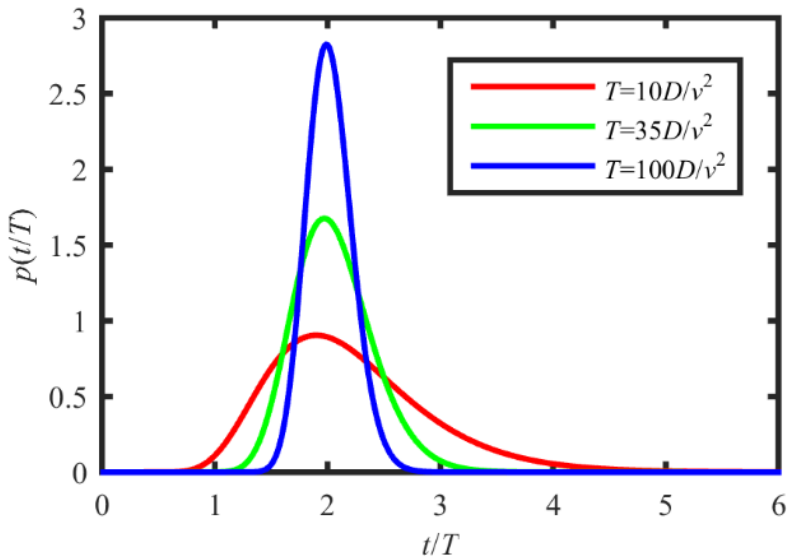

Fig. 4: Probability density function of interval between molecule passages, as given by Eq. (2-11).

The ML estimate of D is the value of D for which Eq. (2-12) is a maximum, which is found by solving $\partial L(D;t_i)/\partial D = 0$, which is given by

$$\frac{\partial L(D;t_i)}{\partial D} = \left(\frac{-1}{2D} + \frac{v^2(t_i - 2T)^2}{4D^2 t_i} \right) L(D;t_i) = 0. \tag{2-13}$$

Solving Eq. (2-13) gives,

$$\hat{D}_i = v^2(t_i - 2T)^2 / (2t_i)\,. \tag{2-14}$$

When R independent measurements t_i are made of the intervals between detections, if each estimate is of equal reliability, the ML estimate from the set would simply be the mean of the individual measurements,

$$\hat{D} = \frac{v^2}{2R} \sum_{i=1}^{R} \frac{\left(t_i - 2T\right)^2}{t_i}\,. \tag{2-15}$$

If the Gaussian approximation in Eq. (2-11) is valid, we have

$$L(D;t_i) = \frac{v}{\sqrt{8\pi DT}} \exp\left[\frac{-v^2(t_i - 2T)^2}{8DT} \right], \quad D \in [0,\infty), \tag{2-16}$$

$$\hat{D}_i = v^2(t_i - 2T)^2 / (4T)\,, \tag{2-17}$$

and for M independent measurements, Eq. (2-14) becomes $\hat{D} = \frac{v^2}{4RT} \sum_{i=1}^{R} \left(t_i - 2T\right)^2$, which is $v^2/(4T)$ multiplied by the variance of the intervals.

The likelihood functions in Eqs. (2-12) and (2-16) are not normalizable (i.e., $\int_0^\infty L(D;t_i)dD = \infty$). However, if we restrict measurement results to those possible when the interval between passages is in the range $T < t_i < 3T$, then the estimate $\hat{D}$ is always

within a finite range $\hat{D} \in [0, D_{\max}]$, where $D_{\max} = v^2 T/4$ if $T >> D/v^2$ and N = 0. If we restrict D to this same finite range, we can normalize the likelihood function, as the integral over the range is now finite,

$$\int_0^{v^2T/4} L(D;t_i)dD = \frac{v^2}{\sqrt{8\pi}} \exp\left[\frac{-(t_i - 2T)^2}{2T^2}\right] + \frac{v^2 |t_i - 2T|}{4T}\left[Erf\left(\frac{|t_i - 2T|}{\sqrt{2}T}\right) - 1\right] = K(t_i). \tag{2-18}$$

Hence the pdf for D confined to this finite range, which allows us to determine the confidence limits of an estimate, is

$$p(D;t_i)dD = \frac{L(D;t_i)dD}{\int_0^{v^2T/4} L(D;t_i)dD} = \frac{1}{K(t_i)} \frac{v}{\sqrt{8\pi DT}} \exp\left[\frac{-v^2(t_i - 2T)^2}{8DT}\right] dD, \quad D \in [0, v^2T/4]. \tag{2-19}$$

By substituting $x = D / D_{\max}$ and $d = |t_i - 2T| / T$, Eq. (2-19) may be put into non-dimensionalized form as $p(x;d)dx = x^{-1/2} \exp\left(-d^2 / 2x\right) dx / K(d)$, where $K(d) = \int_0^{D_{\max}} p(x;d)dx$. Fig. 5 shows non-dimensionalized plots of Eq. (2-19) for several values of $d = |t_i - 2T| / T$, while the inset of Fig. 5 gives an example of how to determine confidence limits for D from the pdf for the case in which $d = 0.3$, corresponding to $t_i = 2.3T$ or $t_i = 1.7T$.

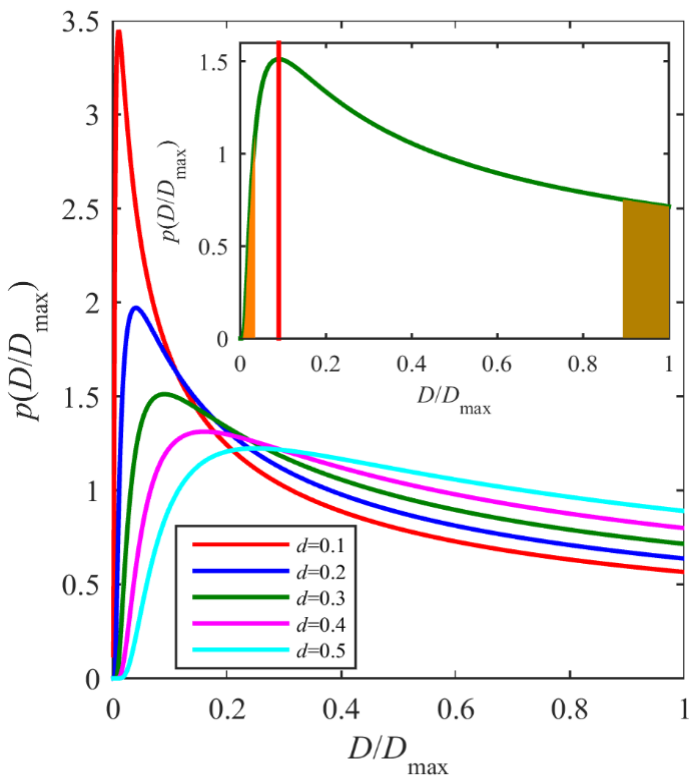

Fig. 5: The pdf of D in non-dimensionalized units, from which the ML estimate of D and its confidence limits are determined.

The ML estimate of $D/D_{\max}$ is the value at which the pdf is a maximum, which for the case of Fig. 5 is $D/D_{\max} = d^2 = 0.09$, consistent with Eq. (2-16). Also, as seen in the inset of Fig. 5, with the prior knowledge that D is in the range $0 \le D \le D_{\max}$ and with a single measurement of $t_i = 2T \pm 0.3T$, $D > 0.039 D_{\max}$ comes with 98% confidence as $\int_0^{0.039} p(x)dx = 0.02$ (orange area in Fig. 5), and $D < 0.864 D_{\max}$ has 90% confidence as $\int_{0.864}^{1} p(x)dx = 0.1$ (brown area in Fig. 5).

We have yet to account for uncertainties in $\hat{D}_i$ that arise when determining the interval between the times of passage of the molecule. To obtain the pdf of the estimated time of passage t_i^e, let's combine the normally distributed timing error $g(t_i^e - t_i, \delta_t)$ with the Gaussian approximation for the pdf of the interval between molecule passages t_i given in Eq. (2-11), i.e.,

$$p(t_i^e)dt_i^e = g(t_i^e - t_i, \delta_t) * g\left(t_i - 2T, \sigma_D\right)dt_i^e, \tag{2-20}$$

where $\left(q * r\right)(x) = \int_{-\infty}^{\infty} q(x - x')r(x')dx'$. As the convolution of two Gaussians is another Gaussian with widths added in quadrature, we have

$$p\left(t_i^e\right)dt_i^e = g\left(t_i^e - 2T, \sqrt{\sigma_D^2 + \delta_t^2}\right)dt_i^e, \quad t_i^e \in (0, \infty). \tag{2-21}$$

As before, by the ML method explained following Eq. (2-12), when a particular measurement result t_i^e is inserted into Eq. (2-21), we get a function that expresses the likelihood of D for the given measurement:

$$L(D;t_i^e)=\frac{1}{\sqrt{2\pi(4DT/v^2+\delta_t^2)}}\exp\left[\frac{-(t_i^e-2T)^2}{2(4DT/v^2+\delta_t^2)}\right]. \tag{2-22}$$

If we confine D to the range $0\le D\le v^2T/4$, we find that the ML estimate of the diffusivity is

$$\hat{D}_i=\begin{cases}0, \text{ for } 0\le\left|t_i^e-2T\right|\le\delta_t, \\ v^2\left[(t_i^e-2T)^2-\delta_t^2\right]/(4T), \text{ for } \delta_t<\left|t_i^e-2T\right|<T.\end{cases} \tag{2-23}$$

Note that if the timing error were not considered, as in Eq. (2-17), it would introduce a small bias to the ML estimate of the diffusivity. On the other hand, if the measurement result is in the range $2T-\delta_t<t_i^e<2T+\delta_t$, simply solving $\partial L(D;t_i^e)/\partial D=0$ would give an out-of-range, negative value for the estimate. With D confined to the range $0\le D\le v^2T/4$, $\int_0^{v^2T/4}L(D;t_i^e)dD=K(t_i^e)$ is finite and hence the likelihood function in Eq. (2-12) may be normalized to find the pdf $p(D;t_i^e)dD=L(D;t_i^e)dD/K(t_i^e)$. Non-dimensionalized plots of $p(D/D_{\max};\left|t_i^e-2T\right|/T)d(D/D_{\max})$ look very similar to the curves in Fig. 5, but are shifted to the left by an amount $(\delta_t/T)^2$ and truncated to be 0 outside the domain $0\le D/D_{\max}\le 1$.

For a dataset of multiple independent measurements, t_i^e, $i=1,2,...,M$, the pdf for D may be found by normalizing the product of the likelihood functions for each of the measurements:

$$p(D;t_1^e,t_2^e,...,t_M^e)dD = \frac{\left[\prod_{i=1}^{M} L(D;t_i^e)\right]dD}{\int_0^{v^2T/4}\left[\prod_{i=1}^{M} L(D;t_i^e)\right]dD}. \tag{2-24}$$

Eq. (2-24) can be evaluated numerically for a given set of measurements, t_i^e, $i = 1,..,M$, and then used to find the ML-estimate $\hat{D}$ and its confidence limits. To facilitate the computation during the SMR process, we multiply Eq. (2-22) by $\sqrt{2\pi}T$ to get

$$L(D;t_i^e)\sqrt{2\pi}T = \left[\frac{D}{D_{\max}} + \left(\frac{\delta}{T}\right)^2\right]^{-1/2} \exp\left\{\frac{-\left[(t_i^e - 2T)/T\right]^2}{2\left[D/D_{\max} + (\delta/T)^2\right]}\right\}, \tag{2-25}$$

for $T < t_i^e < 3T$ and $0 \le D \le D_{\max}$ with $D_{\max} = v^2T/4$. We evaluate the logarithm of Eq. (2-25) for all possible values of $\left|t^e - 2T\right|/T$ (i.e., for $\left|t^e - 2T\right|/T = d_k = k\,\Delta t_W/T$, with $k = 0,1,...,(T/\Delta t_W)$ and Δt_W = 10 μs defined in section 2.2), and we store these in a look-up table, which is given by,

$$s(j,k) = -\left(\ln e_j + d_k^2/e_j\right)/2, \tag{2-26}$$

where $e_j = D_j/D_{\max} + (\delta_t/T)^2$, and $D_j = jD_{\max}/j_{\max}$, $j = 0,1,..., j_{\max}$, $j_{\max} \approx 10000$. As each passage time and interval are estimated, we determine the normalized interval d_k since the previous passage, and we add the corresponding values from the look-up-table $s(j,k)$ to an array $S(j)$. At the end of the recycling, we subtract the maximum of $S(j)$ from each element of the array (to effect scaling to avoid numerical underflow), take the antilogarithm, and normalize (divide by the sum) to find the pdf of Eq. (2-24).

The MATLAB program in the Appendix is the code for implementing this calculation. In Fig. 6, we plot an example of the evolution of Eq. (2-24) when simulating SMR. The simulation parameters are as in Table 1 of Chapter 3, except there is only one molecule with $D = 4.90 \times 10^{-11}$ m^{2}s^{-1}, which is indicated by the red vertical line; the concentration of the reservoir is zero, and photobleaching efficiency is zero. The times of passage of the molecule are found by method 4, where the timing error is taken to be 1.43×10^{-4} s. In this example, after 200 recycles, the ML estimate found from the peak of the pdf is $D = 4.66 \times 10^{-11}$ m^{2}s^{-1}. Confidence limits for the ML estimate may be determined from the pdf, for example, with 95% confidence, D is within a range of (–17.4, +22.7)% of the ML estimate (i.e., D is in the range $(1–0.174)\hat{D}$, $(1+0.227)\hat{D}$). The actual value is $1.05\hat{D}$, which is indeed within the 95% confidence interval. To illustrate an alternative way for finding D (albeit without finding the pdf and confidence limits), the inset of Fig. 6 shows a histogram of the intervals between passages, which have a standard deviation of 7.18×10^{-3} s and a Gaussian with this same standard deviation, which by Eq. (2-14), gives $D = 4.98 \times 10^{-11}$ m^{2}s^{-1}. The timing error δ_t could be considered by subtracting it in quadrature from the standard deviation, but in this case gives only 2% bias.

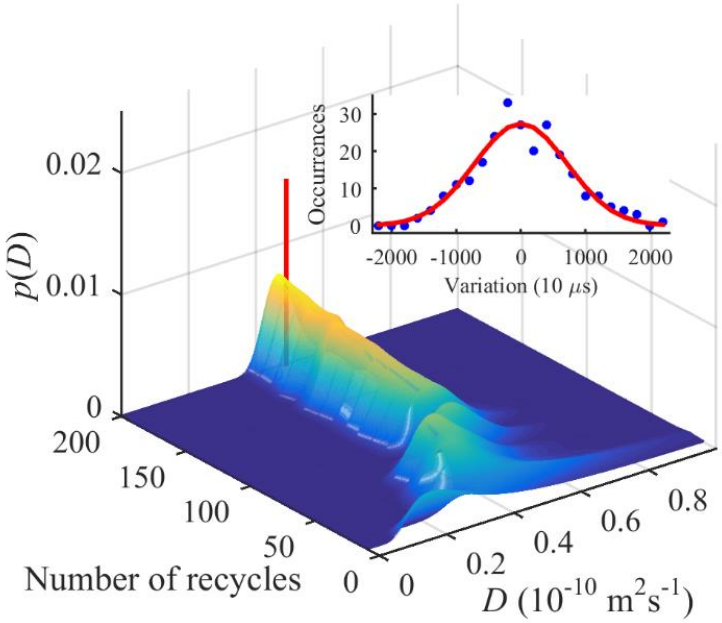

Fig. 6: Evolution of the probability density function of diffusivity *D* as a single molecule is recycled up to 200 times.

CHAPTER 3: SIMULATION RESULTS FOR SINGLE-MOLECULE RECYCLING

In this chapter, we present simulation results and demonstrate that single molecules with different diffusion coefficients can be resolved by SMR.

3.1 Simulation of single-molecule recycling

Simulation results are presented for the parameters listed in Table 1, set to model experiments by Ref. [23]. The molecules are dsDNA13mer (double-stranded 13-base oligomers of DNA) labeled with ATTO 532, which has a peak absorption at 532 nm and emission centered at 553 nm. The simulated experiment times are 1,000 s, while the execution times (including all analyses) are typically ~500 s on a 2.6 GHz 2×2-core Intel Xenon CPU desktop PC with 20 GB of RAM.

In Fig. 7, we show predicted results if a matched digital filter is implemented for improved photon burst detection. The left graph presents the histogram of times between passages with method 1. The curve in the graph is similar to that in the Fig. 3 of Ref. [15]. The right graph shows the histogram of times between passages with method 4. The height of the distribution in the right graph is higer than that in the left graph, which indicates method 4 is more efficient in detecting the photon bursts.

In simulations using the parameters of Table 1, we find that SMR usually continues for only a small number of recycles—for example, when using method 1 (method 4) of section

Table 1: Parameters used in MC simulations.

Parameter	**Value**	**Units**	**Notes**
Laser power (continuous)	98	μW	**1**
Beam waist, ω_0	0.96	μm	**1**
Laser wavelength	532	nm	**1**
Background count rate	600	s^{-1}	**1**
Nanochannel cross-section, A	2.925×10^{-13}	m^2	**1**
Reversal delay, T	30	ms	**1**
Absorption cross section	4.4×10^{-20}	m^2	**2**
Fluorescence lifetime	3.8	ns	**2**
Fluorescence detection efficiency	8.0×10^{-3}		**3**
Triplet crossing efficiency	1.0×10^{-3}		**4**
Triplet lifetime	1.0	μs	**4**
Photobleaching efficiency	1.0×10^{-6}		**5**
Diffusion coefficient, D	9.8×10^{-11}	m^2s^{-1}	**6**
Flow speed, v	3.4×10^{-4}	$m\ s^{-1}$	**6**
Concentration in reservoirs, C	0, 10^{-11}	M	**7**
SPAD timing jitter	127	ps	**8**
SPAD dead time	40	ns	**8**
SPAD afterpulse probability	5×10^{-3}		**8**
SPAD afterpulse decay time	100	ns	**8**
Grid resolution, Δx, Grid length	0.01, 100	μm	**9**
WSS width, σ_t	1.5	ms	**10,11**
WSS threshold	1750		**10,12**

Table 1. Continued.

Notes: 1: This parameter is taken from Ref. [19] (main paper or sup. info. p. 9). 2: This is for Atto 532 fluorophore (https://www.atto-tec.com/attotecshop/product_info.php?language=en&info=p102_ATTO-532.html). 3: The fluorescence collection and detection efficiency is typically 1–8 % for a high-efficiency single-molecule microscope and a fluorophore with high quantum efficiency [2], but here it is decreased to give 1 ms binned photon bursts with 50 kHz peaks, comparable to the summed peaks of Fig. 2 in Ref. [19]. 4: This is a typical value for many fluorophores. The lifetime is a typical value for triplet quenching by oxygen in solution. 5: This is an estimated value for a fluorophore with good photostability [23], such as Atto 532, in water; by comparison, rhodamine in water is 5.0 × 10–6 [42]. 6: This is for 13-mer dsDNA labeled by Atto 532 [19]. 7: This is a typical value needed to keep the probability of an invader molecule low, while the mean time needed to load a new molecule, 1/(103 NA A C v), is still quite fast (1.7 s). 8: Typical parameters for SPADs in our lab [23]. 9: Simulation parameters. 10: Only used if photon bursts are detected by the WSS method. 11: See section 3, second paragraph; the ideal width is $\omega_0/(2v)$ = 1.41 ms. 12: Obtained from Fig. 1.

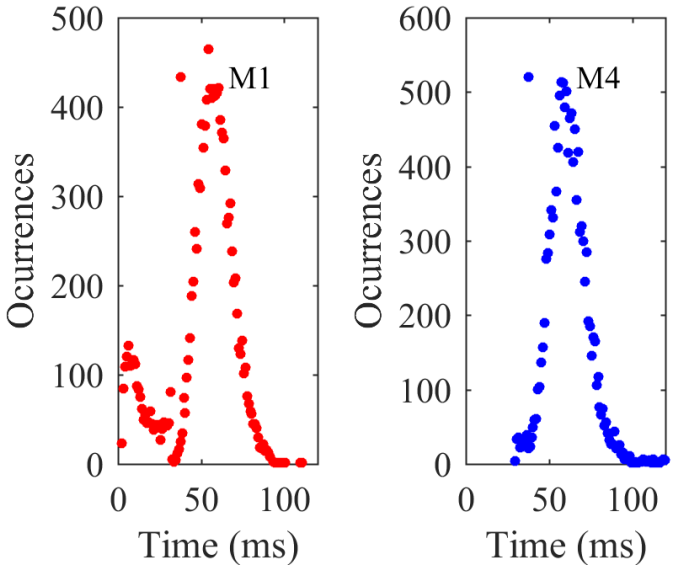

Fig. 7: Histograms of times between passages.

4 and algorithm (a) of Fig. 3 (reload if an unexpected molecule passage is detected), with a maximum number of missed detections of $M = 4$, on average, a molecule is recycled only ~14 (~4) times before the SMR terminates and a new molecule is loaded, while only very occasionally is a molecule recycled for hundreds of times. We find that the SMR terminates after a small number of recycles even if photobleaching and triplet crossing are set to zero and if there is no possibility of an invader molecule. On inspection, as explained below, we find that the terminations are due to statistical outliers in the diffusion trajectories leading to poorly timed flow switching.

In the experiments from which the parameters in Table 1 were taken, the reversal delay T was chosen to be relatively long and the electrophoretic flow speed v relatively low in order to increase the diffusional spread $\sigma_D = \sqrt{4DT}/v$ in the pdf for the interval between molecule passages, which is given in Eq. (2-11) and from which the diffusivity is determined. However, a decrease in the flow speed also increases the effects of diffusion during each transit of the molecule through the laser focus. To mitigate these effects, in the experiment, the beam waist was increased to 0.96 μm by under-filling the microscope objective pupil. Nevertheless, the flow residence time, which is the time it takes for a molecule beginning at the origin to flow beyond the beam waist, is $\tau_F = \omega_0/v = 2.82$ ms, whereas the diffusional residence time, which is the average time it takes for a molecule beginning at the origin to diffuse beyond the beam waist, is $\tau_D = \omega_0^2/(4D)$ = 2.35 ms. Since $\tau_F > \tau_D$, the flow is still slower than the effective speed due to diffusion, so much of the time, the molecule diffuses in and out of the laser focus during each transit. As a

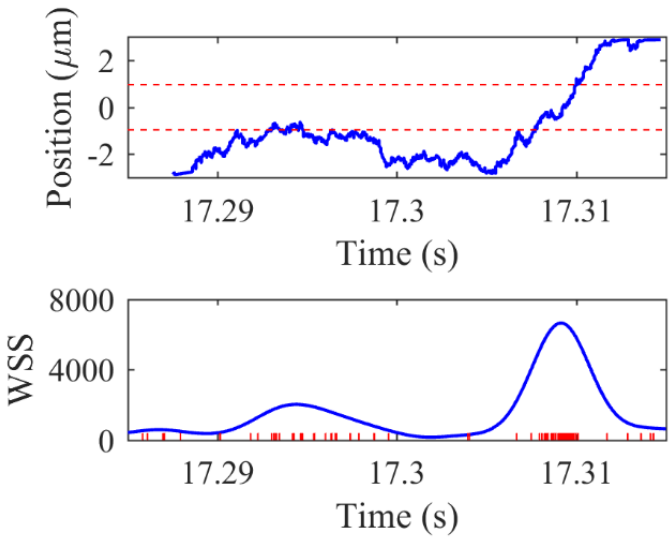

Fig. 8: Example of the trajectory of a molecule as it transits the laser focus.

consequence, the WSS often results in multiple peaks, as seen in the example in Fig. 8, which shows the trajectory of a molecule, the times of photons, and the corresponding WSS, which in this case has two peaks. In Fig. 8, solid blue line in top graph is the trajectory of the molecule; the times of detected photons are short red vertical lines in bottom graph; the corresponding weighted sliding sum is solid blue line in bottom graph; the red dashed lines in the top graph represent the beam waist of the laser focus.

If the second peak in the WSS were interpreted to be due to an invader molecule, the SMR would be terminated and a new molecule would be loaded. This possibility can be avoided by ignoring peaks that closely follow another, or by using such peaks to adjust the scheduled time for the next flow reversal without also changing the direction, as accomplished by the options (b) or (c) near the end of the flow diagram in Fig. 3. On the down side, these algorithms limit the capability to distinguish invader molecules. On the down side, such algorithms limit the capability to distinguish invader molecules. In any case, even with algorithms (b) or (c), the SMR is often disrupted when a molecule by chance diffuses against the flow so that it would arrive at the laser focus late, after an automatic recycle event is scheduled, as shown in the example trajectories of Fig. 9.

In the examples in Fig. 9 A, a molecule passage is detected at time $t = 0.9899$ s and the flow is reversed after $T = 30$ ms, i.e., at $t = 1.0199$ s. As shown by the red line in Fig. 9 A, if automatic recycling is not used (i.e., maximum number of missed detections $M = 0$), the flow direction is held constant until the next passage is detected, which happens to occur at $t = 1.0857$ s. Although it has a low probability, the molecule has diffused against the

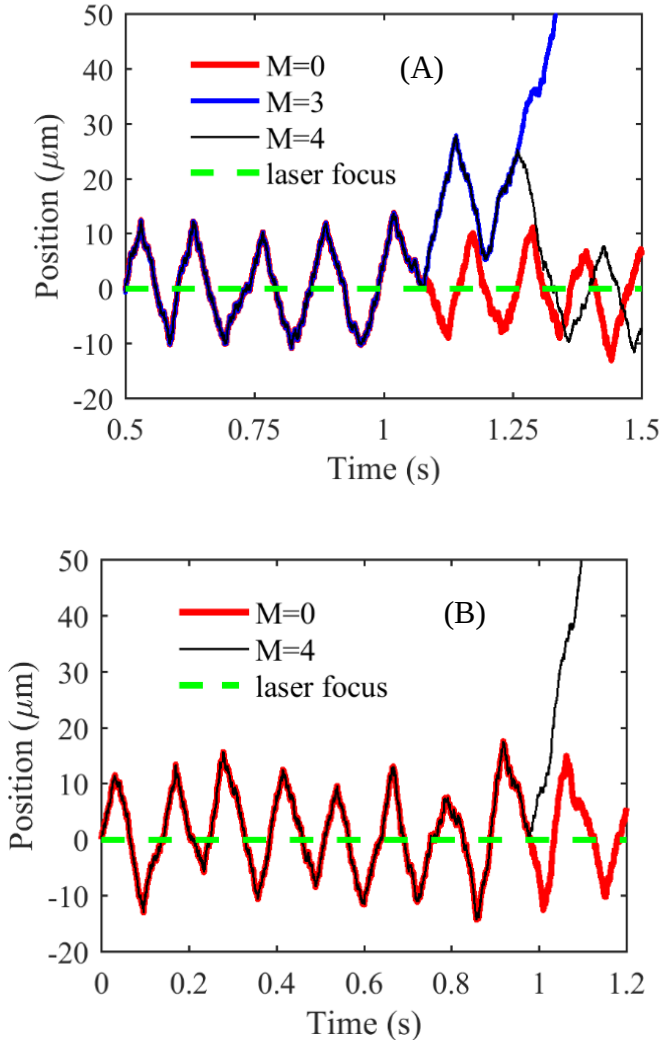

Fig. 9: Trajectories of a molecule undergoing SMR, with parameters from Table 1.

flow so that the interval between detected passages is greater than $3T$ (90 ms). On the other hand, automatic recycling is needed because triplet crossing and other stochastic photon detection cases sometimes result in a missed detection. With automatic recycling and maximum number of missed detections $M = 3$ (blue line in Fig. 9 A), after the flow reversal at $t = 1.0199$ s, the flow is reversed again after $2T = 60$ ms, i.e., at $t = 1.0799$ s, before the molecule has passed through the focus, and hence SMR is disrupted. Two more automatic flow reversals occur, but the molecule diffuses further from the laser focus and a passage is not subsequently detected, and hence SMR is terminated and a new molecule is loaded. If automatic recycling is used but M is even (black line in Fig. 9 A for $M = 4$), there will be a period of missed detections and eventually the molecule will return to pass through the laser beam so SMR will not be terminated. On the other hand, SMR can be terminated even if automatic recycling uses an even number for M, as illustrated in Fig 9 B. Here, for the black line for $M = 4$, a molecule passage is detected at $t = 0.8892$ s, the flow is automatically reversed at $t = 0.9192$ s, but the molecule diffuses against the flow causing an unexpected photon burst very soon after, centered at $t = 0.9777$ s. As this could be due to an invader molecule, SMR is terminated and the flow direction is held steady to reload a new molecule.

To increase the number of recycles, one could reduce the probability that SMR becomes interrupted by occasional passage times that occur out of limits by choosing parameters that give a greater probability p that the interval t_i between molecule passages is within limits $T < t_i < 3T$. The probability p may be obtained by referring to Fig. 4 and Eq. (2-11),

and is approximately given by $p \approx \int_T^{3T} g(t-2T,\sigma_D)dt = erf\left(T/(\sqrt{2}\sigma_D)\right)$, where $erf(x)$ is the Gaussian error function. For example, if we wish to recycle at least r = 200 times with 90% probability of no interruption, as the probability that r successive intervals are all within limits is p^r, we require $p^{200} > 0.9$, so $p > 0.99947$, and hence $T/(\sqrt{2}\sigma_D) > 2.4514$ (= $erf^{-1}(0.99947)$), which gives $v^2T/D > 48$. By comparison, for the parameters of Table 1 and for the middle curve in Fig. 4, $v^2T/D \approx 35$.

3.2 Measuring diffusivities and resolving different species

We use the ML method from the last section to measure the diffusivities of individual molecules. Simulated examples of measuring the diffusivity of dsDNA13mers labeled with ATTO 532 are shown in Fig. 10. The parameters of the simulation are as those in Table 1. The molecules in the graph are all cycled more than 5 times.

By measuring the diffusivities of different molecules mixed in one solution, biomedical molecules with different diffusion coefficients, but labeled with the same fluorescent probe, can be resolved by the SMR technique. In Fig. 11, dsDNA15mers with diffusion coefficient 0.98×10^{-10} m^2s^{-1} and dsDNA13mers with diffusion coefficient 1.3×10^{-10} m^2s^{-1} can be clearly distinguished if the number of recycles is above 200. The result demonstrates that single molecules with diffusion coefficients differing by less than a factor of two could be resolvable if the number of recycles is sufficiently high. The simulated experiment time for Fig. 11 is 2000 s.

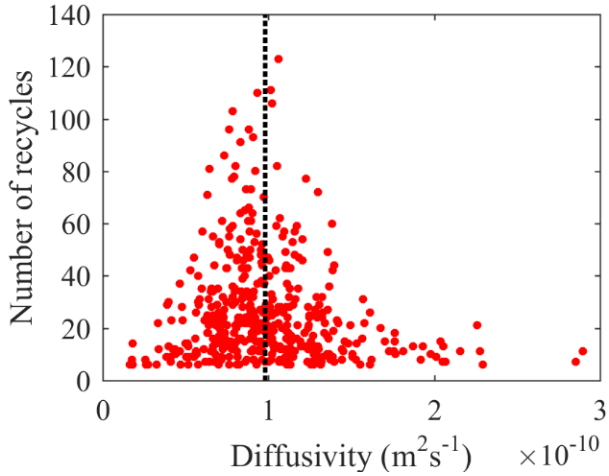

Fig. 10: Plot of ML estimated diffusivities versus numbers of recycles.

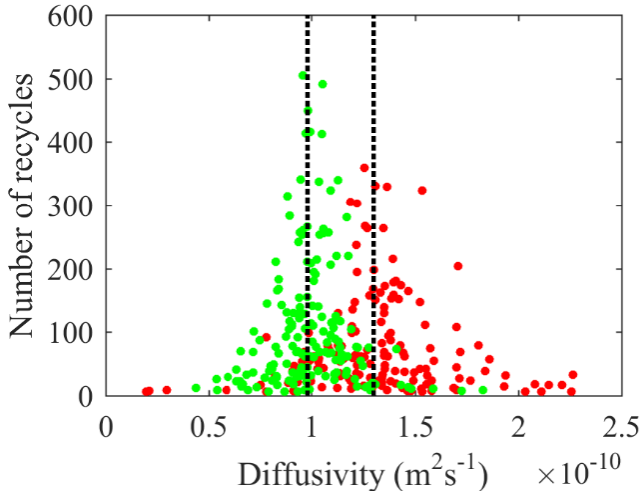

Fig. 11: DNA 13mers and DNA 15mers are resolved by estimating their diffusivities. The two vertical lines are diffusivities of the two species [23].

CHAPTER 4: SIMULATION FOR A QUANTUM DOT AND TWO-PHOTON EXCITATION EXPERIMENT

This chapter presents a simulation of fluorescence from a CdSe nanocrystal or quantum dot (QD) based on an Auger-ionization model, which includes photophysics that account for the observed fluorescence intermittency and the "power law" distribution of the "on" and "off" states. We model both one-photon excitation (1PE) and two-photon excitation (2PE) of a single QD and discuss the feasibility of SMR by using 2PE. We then report an initial experiment that demonstrates fluorescence of Rhodamine B with 2PE.

4.1 Energy levels of quantum dots

Ultrasmall CdSe QDs, with a diameter of less than 2 nm, have potential utility as a wide spectrum light source in solid-state lighting applications as they emit white light [43]. They have a very high surface-to-volume ratio with ~70% of the atoms on their surface [40]. In general, QDs are estimated to be ~20 times brighter and ~100 times more stable than traditional fluorescent probes [40]. From the early days of research, CdSe nanocrystals have been found to exhibit a particular characteristic of fluorescence intermittency, in which they switch between "on" (bright) and "off" (dark) states similar to a random telegraph signal [39, 44], which indicates that they have a fundamentally different energy structure than that of dye molecules [39]. The timespans of the "on" and "off" states fluctuate, and a "power law" can be applied to the distributions of the "on" and "off" periods [45, 46]. The power law distribution is peculiar in that the average of the on or off

time depends on the duration of observation, and the statistics are non-ergodic in that the long-time statistics of a single QD differ from the short-time statistics of an ensemble [47]. Furthermore, the exact physical origin of the "power law" distribution is still uncertain [48]. A recently proposed model postulates that electrons and holes tunnel to trap states located at different distances from the core of the QD and that there are variable trapping rates and recovery from the dark state occurs with variable detrapping rates [48]. This model is consistent with the finding that power law statistical behavior is generally associated with complex dynamics. As described below, in this chapter, we combine the works from Ref. [39] and Ref. [48] to model the fluorescence intermittency in a manner that accounts for the observed power-law statistics.

According to Ref. [39], the laser excitation creates electron-hole (e-h) pairs, which will recombine quickly and emit light. This happens until the QD is ionized either thermally or by Auger ionization, by which the electron or the hole is trapped, and the QD subsequently becomes dark. Before the relaxation of the first excited electron, a second e-h pair may be created. A QD with two e-h pairs has a significantly higher efficiency of Auger ionization and hence, in the model of the QD photophysics, the ionization only occurs in the energy level with two e-h pairs. Also, we neglect the probability that more than two e-h pairs are excited. We attribute the period before ionization as the "on" state and the trapped period as the "off" state. Fig. 12 shows the diagram of the photophysics.

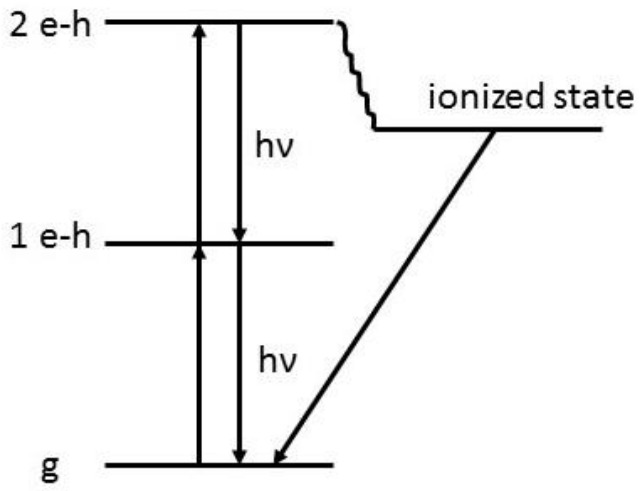

Fig. 12: The diagram of the energy levels of a QD and the transitions between them.

The set of differential equations describing the transitions between the various energy levels is given by [38]

$$\dot{P}_0 = -W_1 P_0 + \frac{P_1}{\tau_1}, \tag{4-1}$$

$$\dot{P}_1 = W_1 P_0 - \left(W_2 + \frac{1}{\tau_1} \right) P_1 + \frac{P_2}{\tau_2} + \frac{P_+}{\tau}, \tag{4-2}$$

$$\dot{P}_2 = W_2 P_1 - \left(\frac{1}{\tau_2} + \frac{1}{\tau_A} \right) P_2, \tag{4-3}$$

$$\dot{P}_+ = \frac{P_2}{\tau_A} - \frac{P_+}{\tau}, \tag{4-4}$$

$$P_0 + P_1 + P_2 + P_+ = 1, \tag{4-5}$$

where $P_{0,1,2}$ are probabilities that a QD is in an energy level bearing zero, one, and two e-h pairs, P_+ is the probability that a QD is in an ionized state, $\frac{1}{\tau_A}$ is the rate of Auger ionization, $\frac{1}{\tau}$ is the rate of returning from a trapped state, and $W_{1,2} = \sigma_{1,2} I / \hbar\omega$ is the excitation rate for the levels with 1 or 2 e-h pairs, where $\sigma_{1,2}$ are the absorption cross sections for exciting these states, and I is the light intensity. However, as discussed in the section below, as the trap states may occur at a range of distances from the core of the QD, the rates $\frac{1}{\tau_A}$ and $\frac{1}{\tau}$ are themselves random.

4.2 Simulation of photokinetics for a single quantum dot

An initial simulation of fluorescence from an immobilized QD with 1PE was executed in order to generate results with on/off statistics similar to those from an experiment on ultrasmall white-light QDs [40]. Table 2 gives the parameters used in the simulation.

In Table 2, the laser power, beam waist, and wavelength are from Ref. [40], in which the experiment uses wide-field excitation of immobilized white-light QDs; the fluorescence detection efficiency is from Ref. [23]; the radiative lifetimes of the 1 e-h and 2 e-h energy levels are taken from Ref. [39]; and the range of lifetimes for τ_A and τ are similar to parameters in Ref. [48], but adjusted to be shorter to model the faster blinking of white-light QDs. Thus in order to model ionization to (or decay from) trap states occurring at a range of distances from the core of the QD, we generate a uniform random number between –8 and –4 (or between –2 and 2), we take the exponential of that random to find the mean τ_A (or τ), and finally we generate an exponentially distributed random with that mean. All other random processes for excitation, emission, and detection of fluorescence are simulated using the methods previously described in Chapter 2.

Fig. 13 presents an example of the results of the simulation for the fluorescence of the QD with 1PE. The binning interval is 10 ms. The criteria to determine the "on" state is that the photon count is greater than 18 within one binning interval, which is the upper limit of the background's photon count. The "on" and "off" states occur irregularly, similar in nature to a random telegraph signal. Fig. 13 shows emission over 100 s, but to gather statistics on the on and off periods, the simulation covers an experiment time of 10,000 s.

Table 2: Parameters used in the 1PE simulation

Parameter	**Value**	**Units**
Laser power (continuous)	25	mW
Beam waist	50	μm
Laser wavelength	400	nm
Fluorescence detection efficiency	0.05	
1 e-h lifetime τ_1	4	ns
2 e-h lifetime τ_2	1	ns
Mean time before ionization τ_A	2×10^{-8} – 2×10^{-4}	s
Ionized state lifetime τ	10^{-2}–10^{2}	s
1 e-h absorption cross section σ_1	1.0×10^{-19}	m^2
2 e-h absorption cross section σ_2	1.0×10^{-19}	m^2

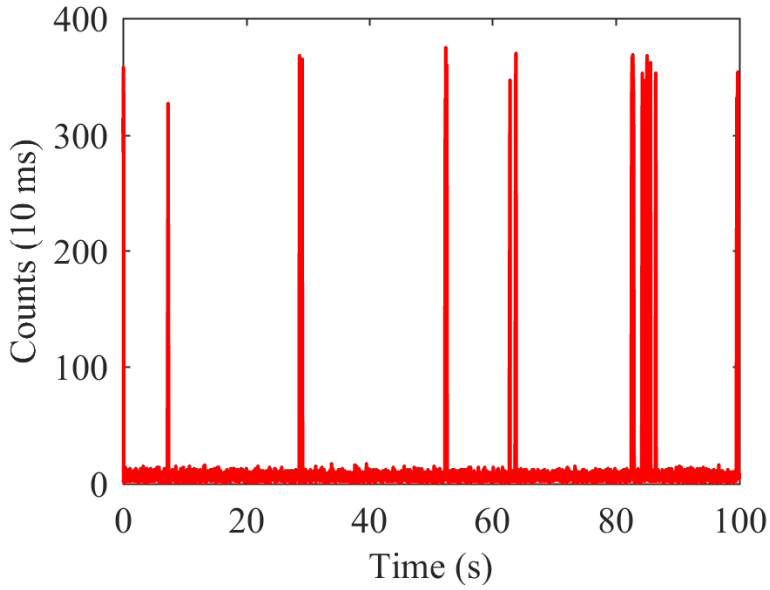

Fig. 13: The photon counts from a single immobilized QD by a simulation of 1PE.

Fig. 14 presents a histogram of the "on" periods and a comparison with experimental results published in Fig. 7 of Ref. [40]. The mean duration of the "on" state is about 120 ms, which is close to that in Fig. 7 of Ref. [40], where white-light QDs are illuminated by 412 nm light. The similarity of the two distributions indicates that the model in the simulation is applicable to explain the photophysics of ultrasmall QDs and is also suitable to explore the feasibility of SMR of such QDs.

If constant decay rates of trapping and detrapping are used, the duration of "on" and "off" states ($\tau_{on/off}$) is expected to follow an exponential distribution [38], but the results of experiments indicate that QDs don't transfer between "on" and "off" states with constant rates [49], and a power law function is applicable to describe the distribution of $\tau_{on/off}$ [45, 46], which follows $p_{on/off} \propto \frac{1}{\tau_{on/off}^{\alpha}}$, where $p_{on/off}$ is the probability that a QD stays in "on" or "off" states for a time $\tau_{on/off}$ and α normally ranges between 1.0 to 2.0. To illustrate the power law distribution, we first simulate with constant values for τ_A and τ of τ_A = 100 ns, τ = 0.8 s, as given in Ref. [39], and we then simulate with random values for τ_A and τ following an exponential distribution over the range of values given in Table 2. Fig. 15 compares the log-log plots of the occurrences of "on" and "off" periods for constant and variable trapping and detrapping rates. The bin steps are exponentially distributed, which gives equally spaced points in the log-log plots. The occurrence of "on" and "off" periods is divided by the subtraction of the two neighbored bin steps to get the counts within time unit.

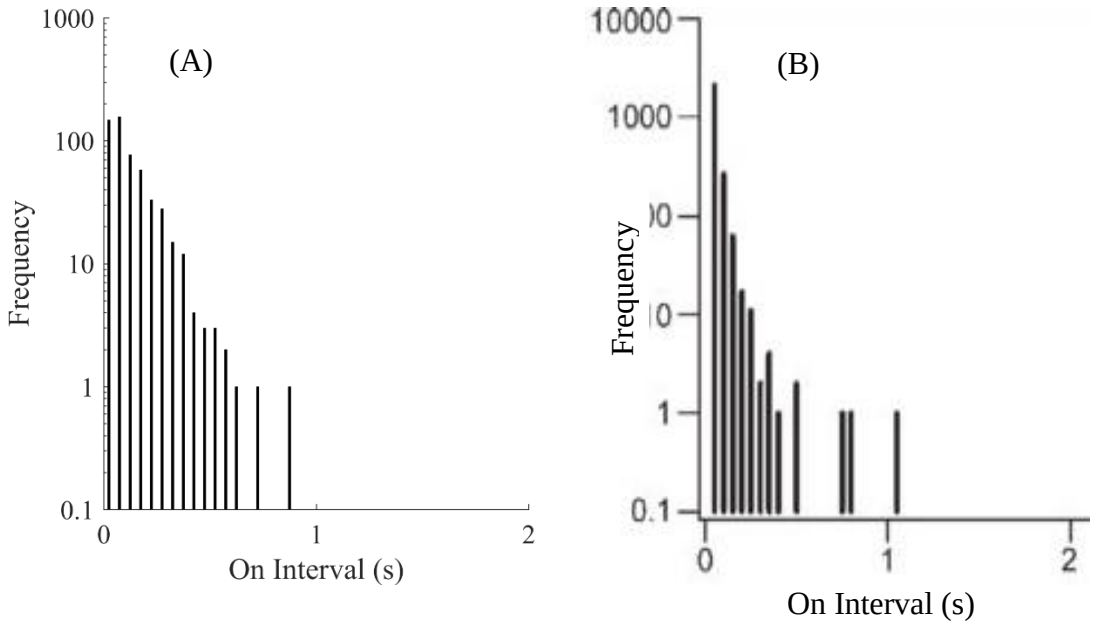

Fig. 14: Comparison of histograms of "on" periods obtained from (A) simulations, and (B) an experiment, as reported in Fig. 7 of Ref. [40].

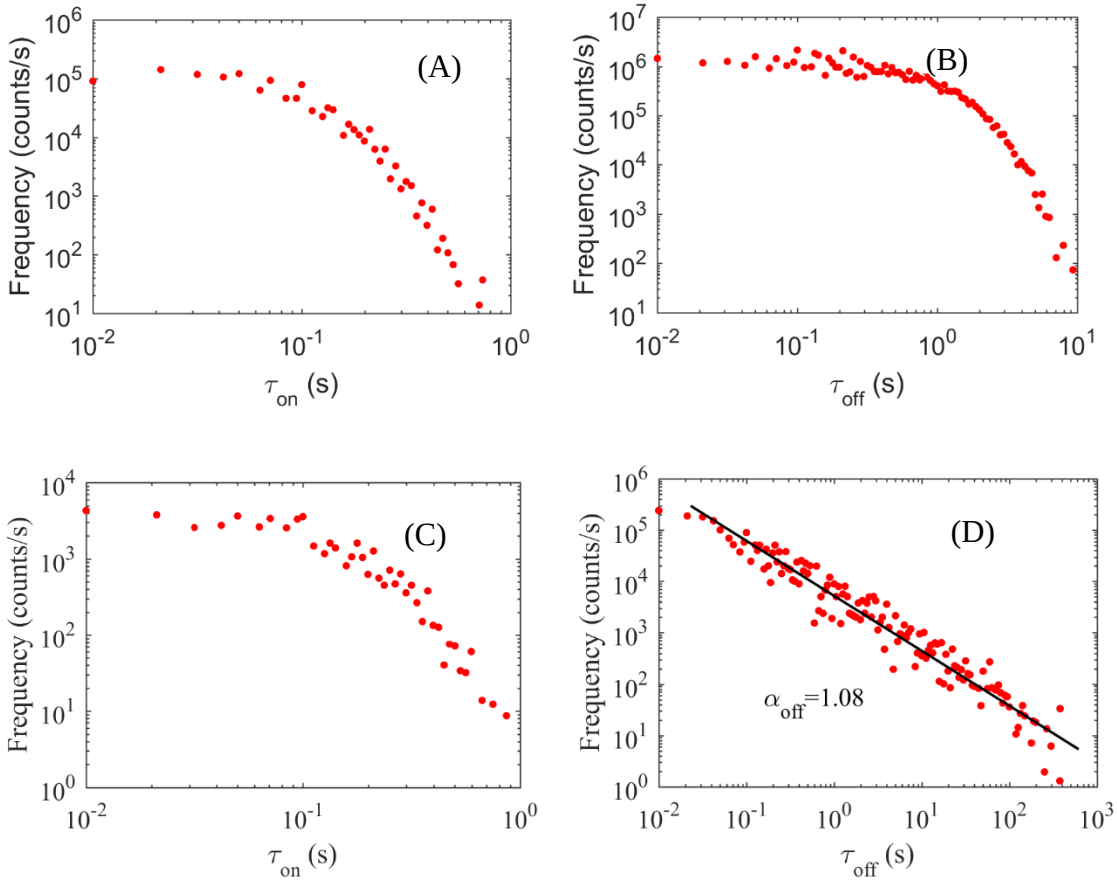

Fig. 15: Occurrences of (A) “on” periods and (B) “off” periods for constant trapping and detrapping lifetimes. Occurrences of (C) “on” periods and (B) “off” periods for variable trapping and detrapping rates.

Fig. 15 A and B are distributions with constant rates, where the nonlinear curves indicate they don't follow a simple power law. Fig. 15 C and D are distributions with variable rates, where the data points in Fig. 15 D fit a straight line and therefore α_{off}=1.08. Because the QD only decays to the trap state after it is stimulated to the state with 2 P-E, the "on" state is less likely to transit to "off" state within a relatively short period of time. Therefore, the occurrences of "on" periods in Fig. 15 C doesn't fit a simple power law.

We next simulate 2PE of QDs using the parameters of the femtosecond laser from our lab. The setup of the laser system will be discussed in the next section. To model 2PE, we use a nonlinear absorption cross section for the excitation of the first e-h pair and a linear absorption cross section for the excitation of the second e-h pair, which is given by $W_1 = \sigma_1 \left(\frac{I}{\hbar\omega} \right)^2$, $W_2 = \sigma_2 I / \hbar\omega$,[50] and $\sigma_1 = 7.9\times10^{-55}\,\mathrm{m^4 s}$, $\sigma_2 = 2.0\times10^{-22}\,\mathrm{m^2}$ [51].

The laser power in our lab is 0.5 mW, the beam waist is 0.17 μm, and the laser wavelength is 812 nm. Fig. 16 A illustrates the photon counts for 2PE of QDs. Fig. 16 B and C show the occurrences of "on" and "off" periods. The plot in Fig. 16 C follows the power law, and α_{off}=1.03. Because the "on" state can last for more than 10 ms, we should be able to recycle a single QD using 2PE.

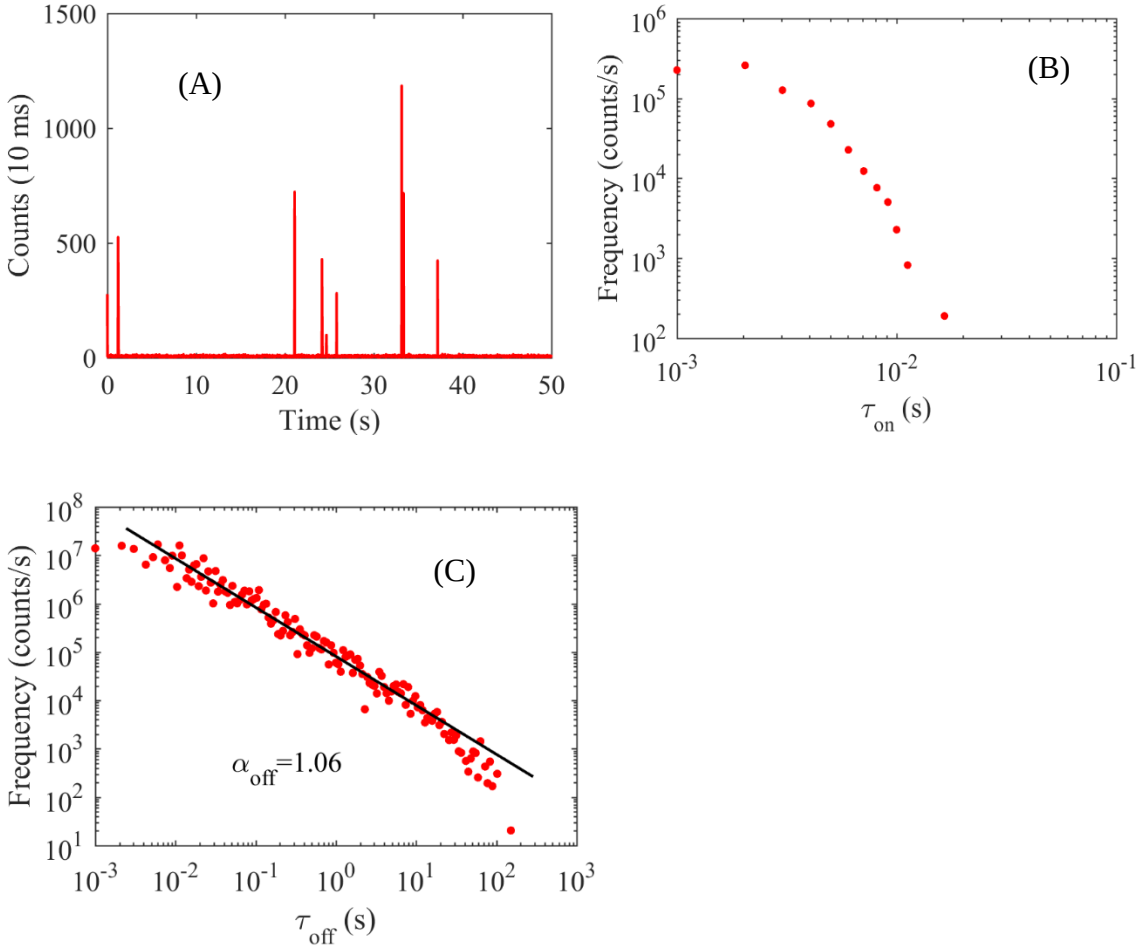

Fig. 16: (A) Photon counts of single QD by a simulation of 2PE. (B) Occurrences of "on" periods. (C) Occurrences of "off" periods.

To simulate SMR of a single QD with 2PE, we estimate the diffusivity of a 2 nm QD using the Stokes-Einstein relation, which is given by $D = \frac{kT}{6\pi\gamma r}$, where k is the Boltzmann constant, T is the room temperature, γ is the dynamic viscosity of water, r is the radius of the QD, then $D = 2.4\times10^{-10}$ m^2s^{-1}. To reduce the probability that the molecule diffuses in and out of the laser focus during each transit, we consider making the diffusional residence time two times of flow residence time, which gives $v_F = 1.1\times10^{-3}$ ms^{-1}. Over the course of a simulated 1000 s experiment, the maximum number of recycles is 31. This is lower than that required for measuring the diffusivity with 10% uncertainty, so it would be difficult to measure a QD's diffusivity by SMR. The histogram in Fig. 17 A shows that most of the QDs are recycled less than 20 times. There are missed detections due to blinking during SMR, as shown in Fig. 17 B. Nevertheless SMR would enable prolonged observation of a single QD freely diffusing in a liquid environment.

4.3 Two-photon excitation experiment

We set up a laser system and preliminary experiment to look into the possibility of SMR of a single QD with 2PE. The laser system consists of a KML femtosecond Ti-Sapphire laser (76 MHz, 40 fs, 812 ± 27 nm, 240 mW) pumped by a SpectraPhysics Argon ion laser and a Biophotonics Femtojock pulse shaper to precompensate the chirp induced at the microscope objective. A photograph of the system is shown in Fig. 18 A.

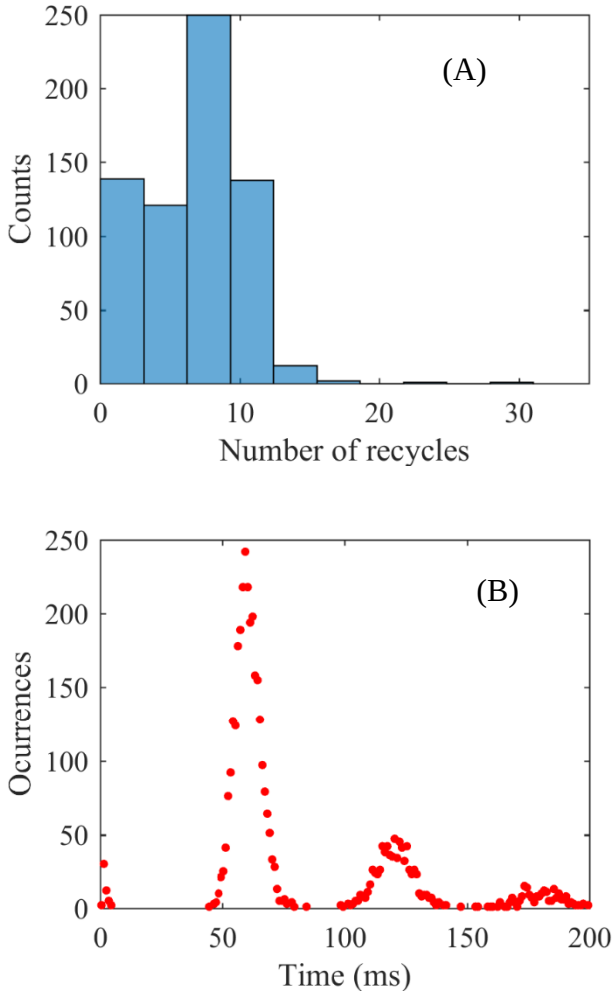

Fig. 17: (A) Histogram of a single QD's number of recycles before it leaves recycling.

(B) Histogram of times between detections. The minor peaks represent misdetections.

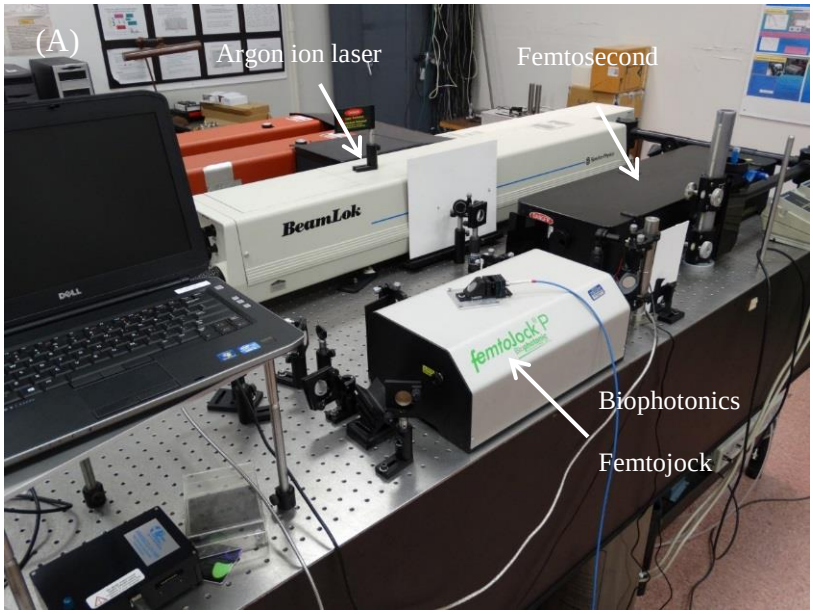

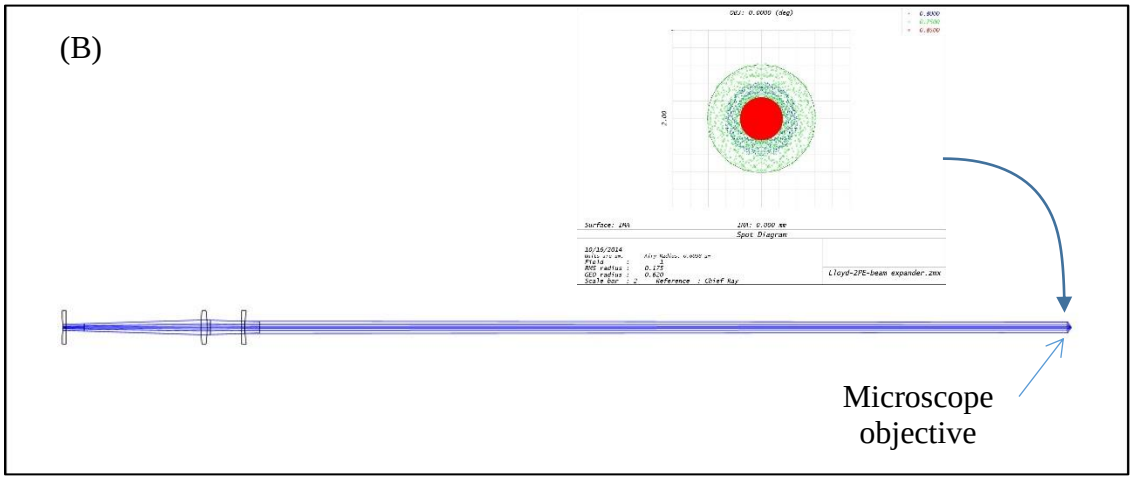

Fig. 18: (A) Laser system for 2PE. (B) Zemax design of beam expander for the femtosecond laser beam (The lenses are Newport KPC019, KBX061, KPC031.) Inset shows the focus is close to diffraction limited.

To adjust the collimation of the beam and expand it to fill the entrance pupil of the objective, it passes through a beam expander composed of three lenses. The beam expander was designed using Zemax optical design software, as shown in Fig. 18 B.

Single-molecule detection and FCS was demonstrated using two-photon excitation of a drop of 1 pM Rhodamine B aqueous solution, with fluorescence isolated using a 430 nm short pass filter and a 670 nm long pass filter. Fig. 19 presents results using a laser power of ~0.5 mW at the sample. The experimental setup can be used for two-photon excitation of QDs, as has been demonstrated by others [52].

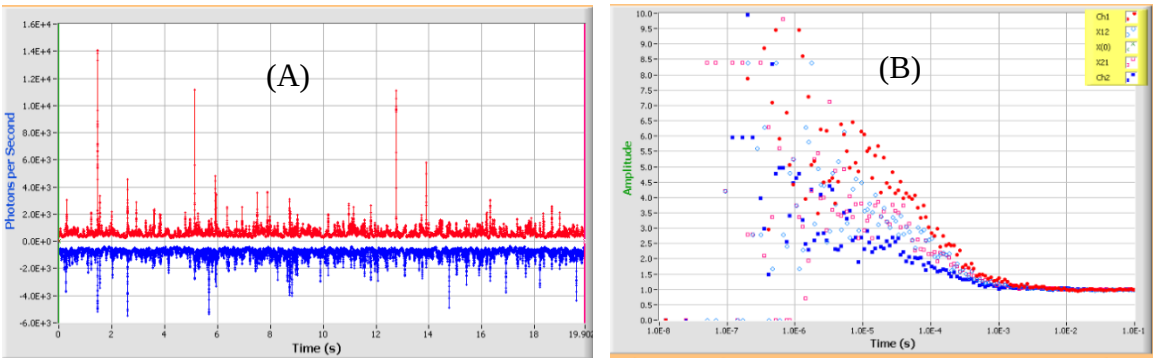

Fig. 19: (A) Photon bursts from single molecules of Rhodamine B, (B) FCS from the two SPADs.

CHAPTER 5: EXPERIMENTAL APPARATUS

This chapter presents the experimental setup for SMR. A schematic of the experimental configuration is shown in Fig. 20. The apparatus includes a laser, a confocal microscope with two single-photon avalanche diodes (SPADs), an electron-multiplying (EM-CCD) camera, a real-time control system implemented in a system of computers, and the microfluidic device. In addition, there is a piezo-driven *xyz* nano-translation unit on which the microfluidic device is mounted. A fluorescently-labeled molecule or bead passes through the laser beam in the microfluidic device, and the fluorescence is collected by the confocal microscope. A beam sampler splits the fluorescence to the EM-CCD and the SPADs. The real-time control system adjusts the voltage across the microfluidic device and/or the piezo translation unit according to the photon counts of the SPADs.

5.1 Laser systems and fluorescence collection

In our lab, beams from different laser systems for either 1PE or 2PE can be adjusted into a custom-built confocal fluorescence microscope through a reconfigurable beam expander. The microscope uses a water-immersion objective with NA 1.2 (Olympus UPLSAP060XW), a 250 mm focal length plano-convex singlet lens as a tube lens for the microscope, and one or more interference filters to isolate the fluorescence from the scattered laser light and Raman-scattered light. For most experiments using 1PE at 647 nm, only one long-pass interference filter is used (Omega 3RD670LP), while for 2PE at ~780 nm, there is also a short pass filter (Semrock FF01-440/SP-25).

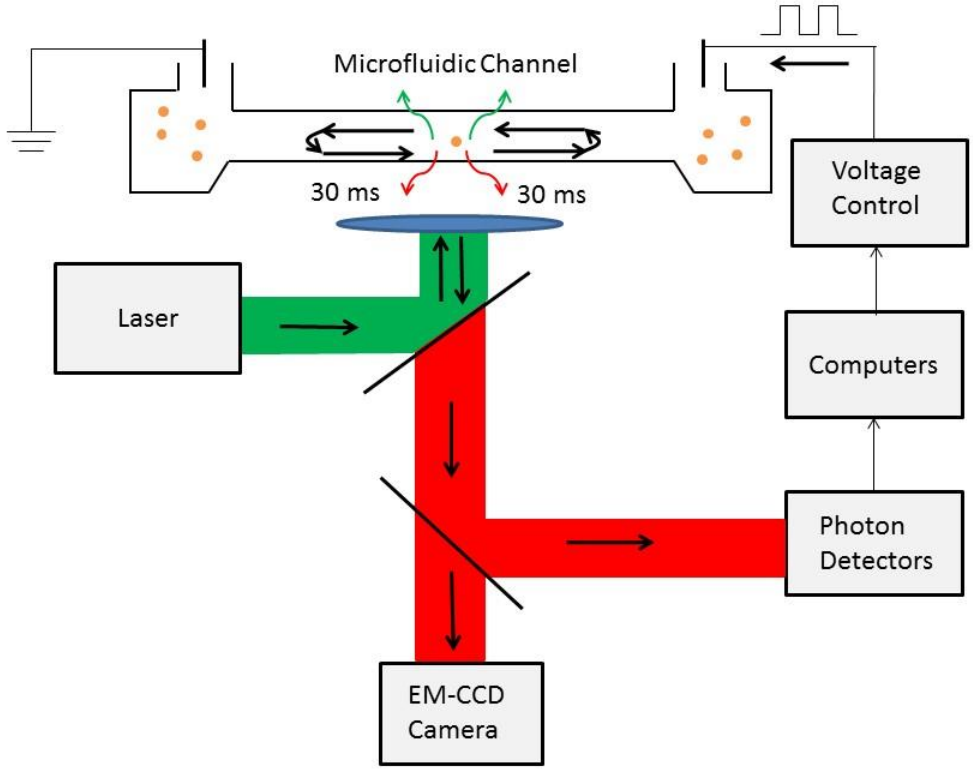

Fig. 20: A schematic of the experimental apparatus for SMR.

After a sample is placed on the observation stage, the laser beam is focused into the sample by the objective so that molecules in the focal volume will emit fluorescence, then the fluorescence from the sample is collected by the same objective. Fig. 21 A shows the beam expander and the microscope. In Fig. 21 B, a beam sampler splits the fluorescence to an EM-CCD camera and the SPADs. For the beam that is split towards the SPADs, the pinhole works as a spatial filter to reject scattered light from outside of the volume of the focused laser beam [53, 54], and a polarization beamsplitter separates photons with different linearly polarized components into two arms, which have lenses to focus the fluorescence onto the SPADs (custom units with detector heads from Perkin-Elmer, Canada, and circuits made by MPD, Italy). As we use different beam waists of focus for nanochannel and capillary microchannel experiments, either a 100-micron pinhole or a 200-micron pinhole is used.

The EM-CCD can visualize fluorescently-labeled beads when they pass through the excitation volume of the laser. In setting up the experiment, we first use a Kohler lens to defocus the laser for wide-field illumination so we can view the microfluidic device on the EM-CCD camera and adjust its transverse position to position the center of the nanochannel where the laser will focus. We then flip up the Kohler lens out of the beam and focus the beam into the channel. As the EM-CCD and the pinhole for the SPADs are parfocal (i.e., they are the same distance from the plane of focus), a clear image of the passing beads indicates that the channel is in the confocal volume and that the SPADs should detect the fluorescence with high signal-to-noise ratio. Fine adjustments to the piezo

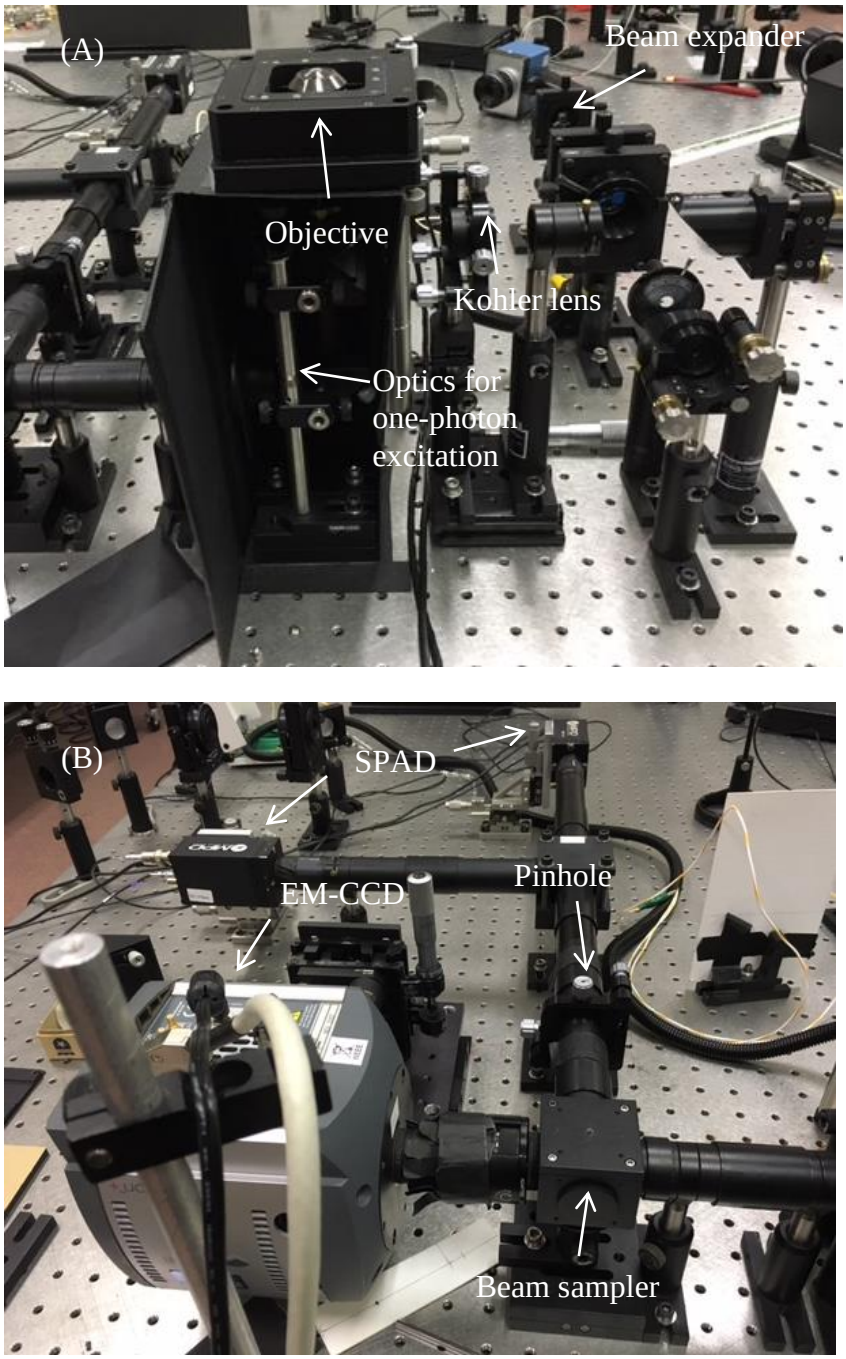

Fig. 21: (A) Configuration of the beam expander and the microscope. (B) Beam sampler, EM-CCD, pinhole, and SPADs.

positioning are then made while monitoring the count rates of the SPADs.

The laser system used for most of the experiments with 1PE consists of a modelocked dye laser (Coherent 700) pumped by a 532 nm laser (Spectra Physics Vanguard). The dye laser uses DCM-special dye and produces picosecond pulses at 76 MHz at a wavelength of 647 nm. To adjust the collimation of the dye laser beam and expand it to give the desired beam size at the entrance pupil of the objective, it passes through a beam expander consisting of three lenses, with placement determined using Zemax optical design software.

In the experiments, we use either nanochannels or capillary microchannels as the containers of single molecules. To make the size of the focus close to the cross-section of the container, we adjust the beam expander to produce a collimated beam with size ($1/e^2$ intensity radius) of either 0.46 mm for the nanochannel experiments or 0.17 mm for the capillary microchannel experiments and then focus the beam with the objective. We will introduce the method used to measure the size of the focus in the next chapter. Fig. 22 shows the beam expander lens placements for the two configurations.

5.2 Real-time control system

To accomplish SMR, we built a control system using LabVIEW Real-Time software. The control system determines the timings of photons detected by the SPADs and applies voltages across the microfluidic device or sends digital signals to adjust the position of the piezo nano-translation unit. The control system includes a NI PCI-7833R FPGA multi-function data acquisition card with digital inputs for signals from the SPADs and analog outputs to provide the voltages to the microfluidics and also a NI PCI-DIO-96 digital

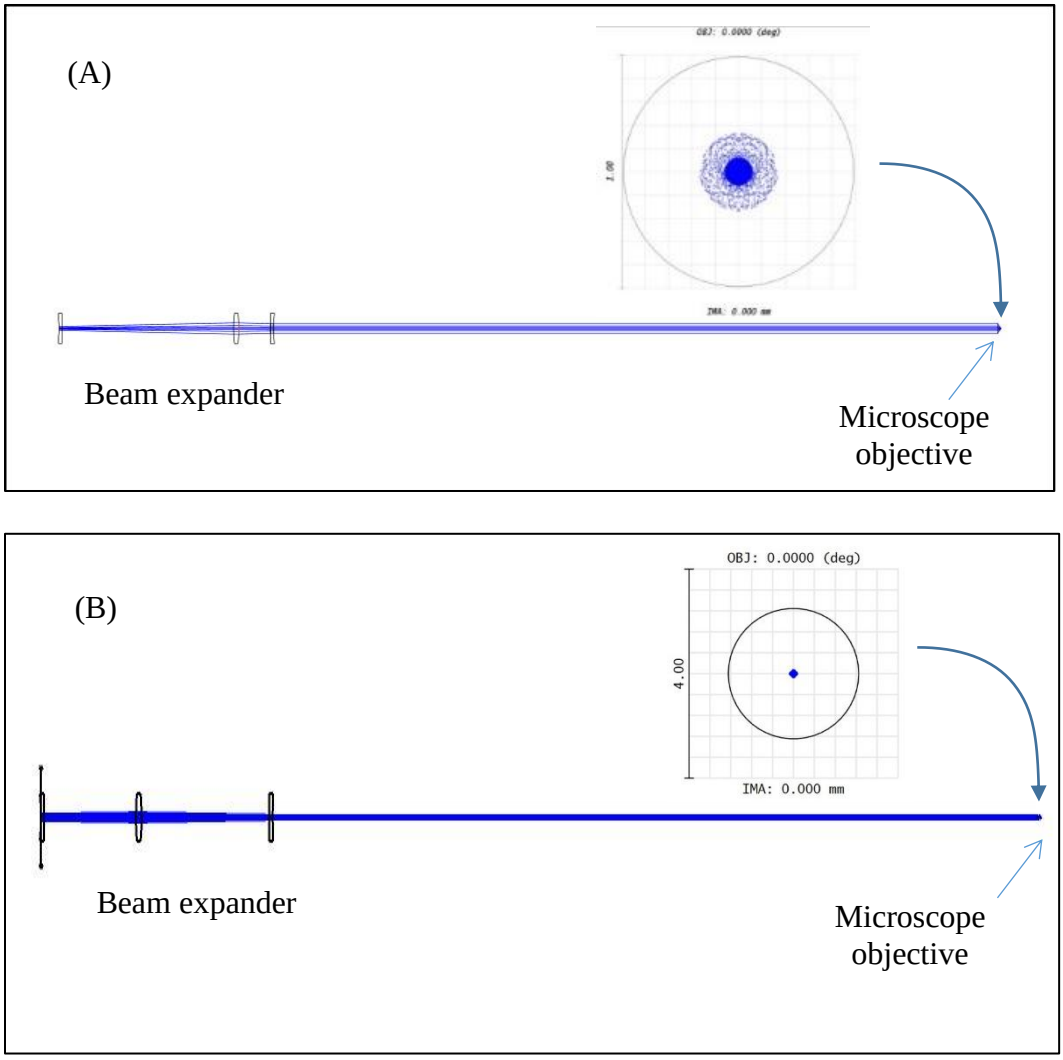

Fig. 22: Zemax design of beam expander to collimate the beam and fill the objective pupil (A) The three lenses are Newport KPC019, KBX064, KPC031, (B) The three lenses are Newport KPC031, KBX064, KPC019).

input/output card that sends digital signals to the PIO (parallel input output) interface of the piezo stage controller. These two cards are contained with a target computer (PC), which is connected to a host PC via the internet. Fig. 23 shows a schematic of the control system.

Photons are detected by the SPADs, which generate transistor-transistor logic (TTL) pulses and their times are determined by the FPGA. We set up a 100 MHz clock on the FPGA and record the count of clock ticks whenever either of the SPADs sends a TTL pulse to the FPGA, thereby recording the timing of the photons with a precision of 10 ns. This data is used only for post-processing, such as for calculation of the autocorrelation function.

We also set up the FPGA to count the TTL pulses from both of the SPADs and to send the count to the target PC every 10 μs. The target PC runs a LabVIEW program that calculates the WSS from the counts received from the FPGA and finds the peaks of the WSS. The times to reverse the flow are determined by adding the reversal delay to the times of the WSS peaks and are sent back to the FPGA, which outputs analog voltages to reverse the flow. Alternatively, the voltages may be held at zero and digital signals sent out from the NI PCI-DIO-96 card so that the sample is translated back and forth using the piezo stage.

We can send a signal from the host PC to the target PC to instruct the control program whether to recycle with voltage or with the piezo stage. For recycling using the piezo, the comands for moving the piezo stage are within a timed loop that is sychronized to a 100 kHz clock signal generated by the piezo controller (PI E-710 console). This

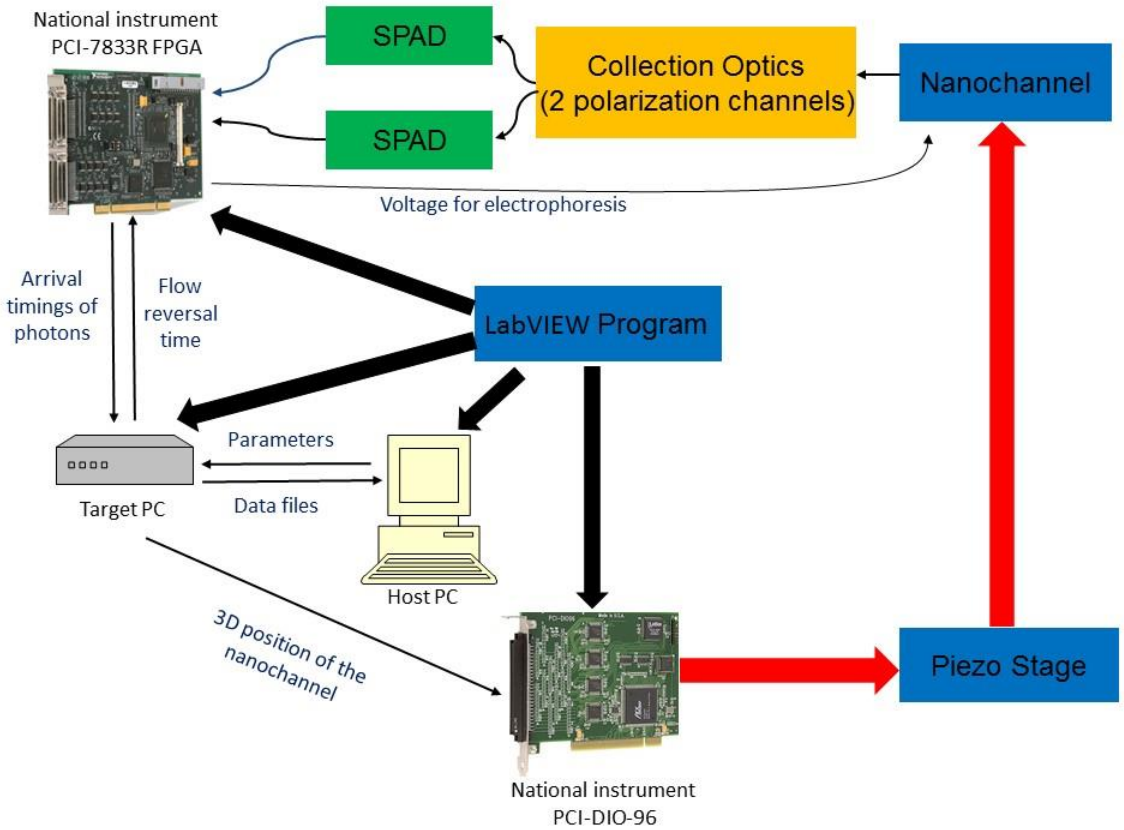

Fig. 23: Control flow of the LabView real-time program.

synchronization is implemented by counting piezo clock pulses at the FPGA and sending data from the FPGA to the target PC at ~10 μs intervals whenever the piezo clock count is incremented. In this way, the real-time program synchronizes its times with the possible motion of the piezo.

For recycling the bead with voltage, there is a small delay between the calculated reversal time and the time at which the analog voltage signals are actually reversed due to the slew rate of the analog outputs. This delay is less than 5 μs and could possibly be accounted for in the calculation. For recycling with the piezo stage, the delay depends on the time to initiate the move, which is usually much longer, but is less than ~2 ms. Details of SMR using the piezo stage are discussed in the next chapter.

The program on the host PC (which is called a virtual instrument or VI) sets up the experiment parameters and plots the count rate of photons, values of the peaks of the WSS, the position of the piezo stage, and histograms of the times between the start of the piezo stage's motion and the peaks of the WSS. From the VI on the host PC, we can send comands to recenter the piezo stage or manually adjust its *xyz* position, which enables us to accurately position the microfluidic device with respect to the laser beam. We can also adjust the threshold for detecting peaks in the WSS and the delay time and other parameters for SMR while observing the experimental outcomes. The program on the target PC consists of the algorithm of SMR, the control of the piezo stage and the output voltage, and the data flows to the host PC. Fig. 24 A presents a part of the block diagram on the target PC, by which the WSS is applied in a time critical loop. Fig. 24 B displays the control of

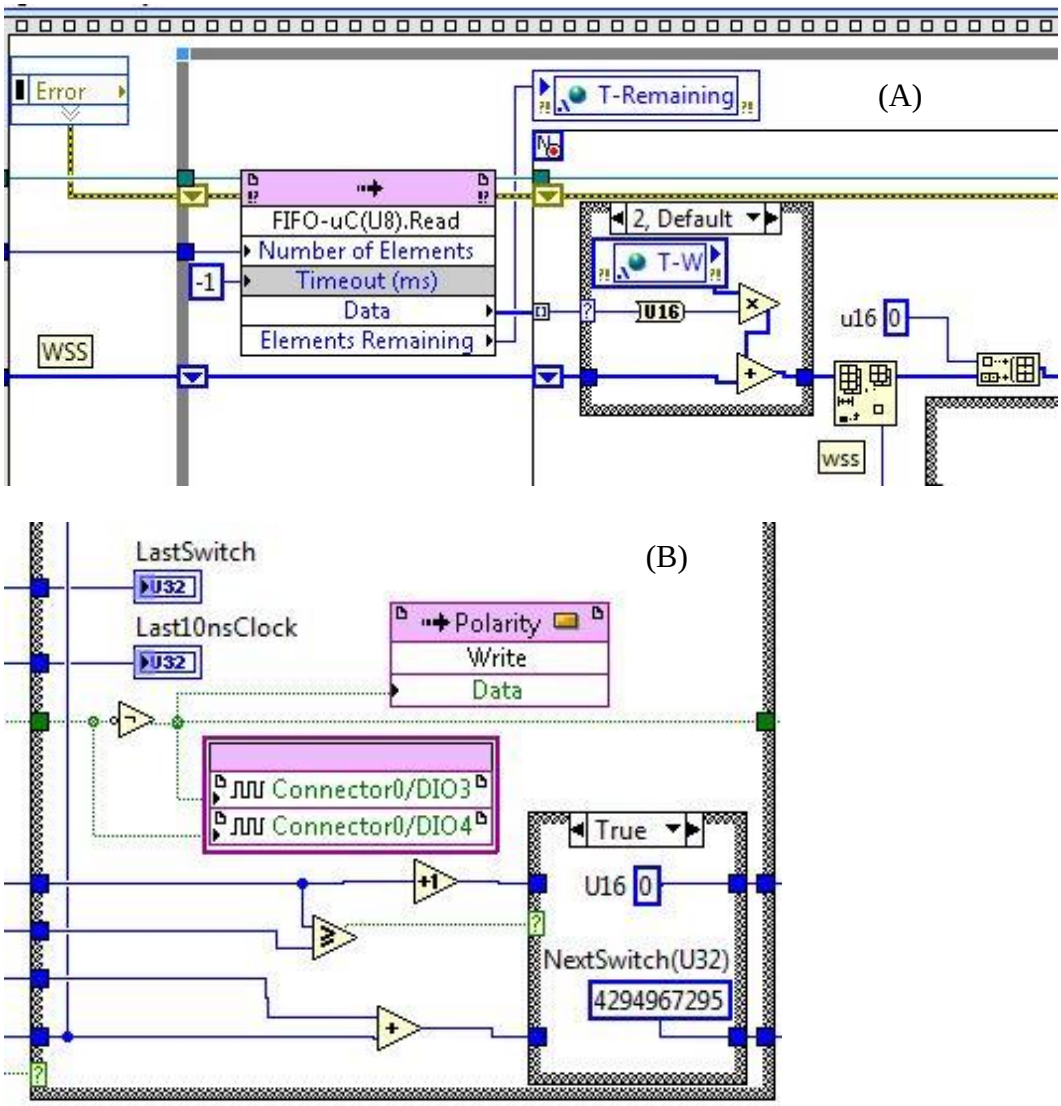

Fig. 24: (A) The block diagram for WSS on the target PC. (B) The block diagram for voltage control on the FPGA.

the output voltage on the FPGA. We send the number of automatic recycles *M* to the program; after the number of misdetections exceeds *M*, it terminates the recycle and holds the voltage fixed in one direction until a burst of photons is detected.

5.3 Microfluidic devices

In the experiment, we use either nanochannels or capillary microchannels as the containers of SMR. Fig. 25 shows the configuration of the nanochannel device. The typical cross-section of our nanochannels is 200 nm × 200 nm. Due to a limited supply of nanochannel devices, in some experiments, we use capillary microchannels, which have an internal diameter of ~ 2 μm, and which are further described below.

In using the nanochannel device, the main problem is that molecules sometimes stick to the surface of the fused silica. This sticking could possibly be made worse by attraction between the charge on the surface of fused silica and the polarity of the molecule. To try to solve the problem, we first used different percentages of methanol in the distilled water based solution, and we tried different fluorescent probes. The best result is from 40 nm Fluospheres® in 50% methanol aqueous solution. Fig. 26 presents an example of a result of SMR in this solution.

We subsequently tried to process the nanochannels with Tween-20 detergent to reduce the non-specific adsorption to the surface as follows [19]: We first make a 0.02% Tween-20 solution in 1×TAE (40 mM Tris-acetate and 1 mM EDTA, usually used as electrophoresis buffer) aqueous solution, where the pH value is around 8.0. Then we use syringes to pump the buffer solution into the microchannel and further into the

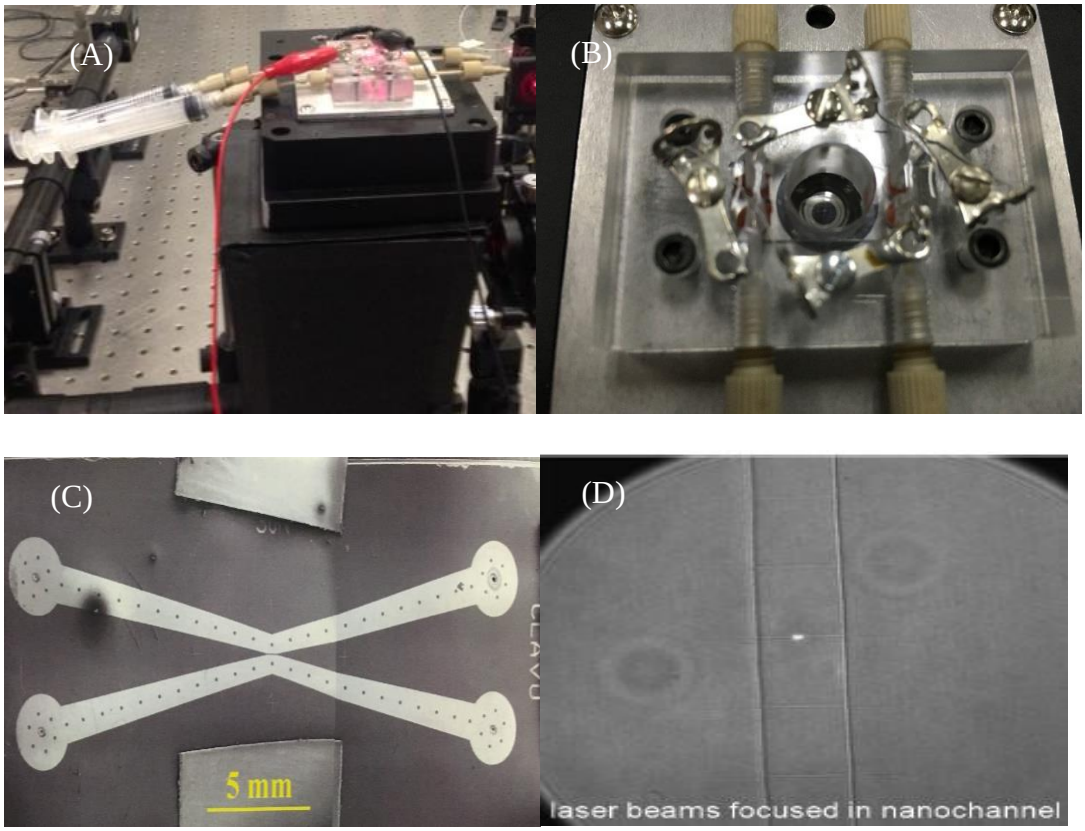

Fig. 25: (A) A nanochannel device is mounted on the confocal microscope, the syringes connect to two microchannels. (B) The housing of the nanochannel device. (C) The contour of the microchannels, which are linked by ten nanochannels. (D) The laser beam focuses into one of the nanochannels. When a molecule goes through the laser spot, the fluorescence is collected by the objective.

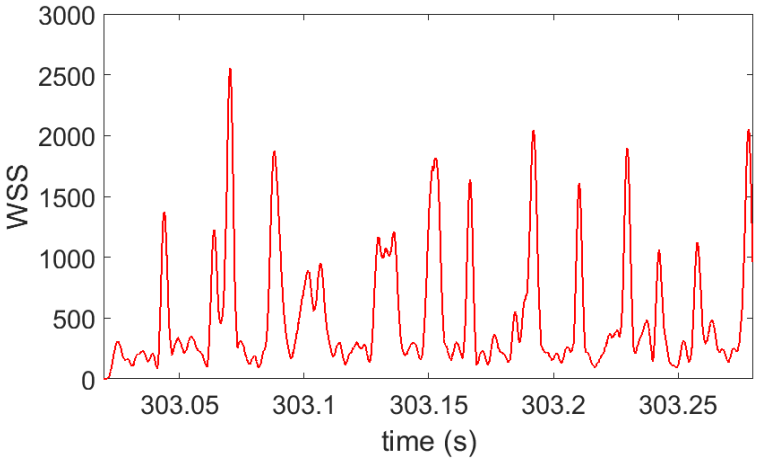

Fig. 26: SMR of 40 nm Fluospheres® in 50% methanol aqueous solution. The reversal delay is 10 ms. The WSS peaks show the molecule can be recycled, but the sticking still appears to be present.

nanochannel, we keep it there for 10 minutes until a layer of Tween-20 forms on the surface of fused silica. To make a working solution, we mix Fluospheres into the buffer and reach the concentration of 10 nM. We then pump the working solution into the microchannel to substitute the buffer solution, connect the device to an external voltage, and start the SMR experiment. The result shows that the sticking is significantly reduced by using Tween-20, and the Fluospheres can be recycled hundreds of times. Fig. 27 shows an example of the photon bursts during SMR as seen by peaks in the WSS. The analysis of the result will be discussed in the next chapter.

We also tried to perform SMR using custom dsDNA molecules in the nanochannel. We purchased 50 bp dsDNA from Life Technologies and labeled it with To-Pro-3 stains. We used 0.5% Tween-20 to process the nanochannel and showed that dsDNA molecules can be moved along the nanochannel by electropheresis, although it seems that randomly occuring temporary adsorption of dsDNA to the surface of the nanochannel causes irregular motion of individual molecules of dsDNA along nanochannel that limits the capability for SMR. Fig. 28 A presents the ACFs of photon counts that shows that the labeled dsDNA molecules move with increasing electrophretic flow for increasing voltage along the nanochannel. The measurement of the flow speed will be discussed in the next chapter. Fig. 28 B presents a plot of the photon bursts acquired during an attempt at SMR. As our supply of nanochannel devices was limited, in some experiments we used microchannel devices, which we made from fused silica capillary (Molex TSP002150).

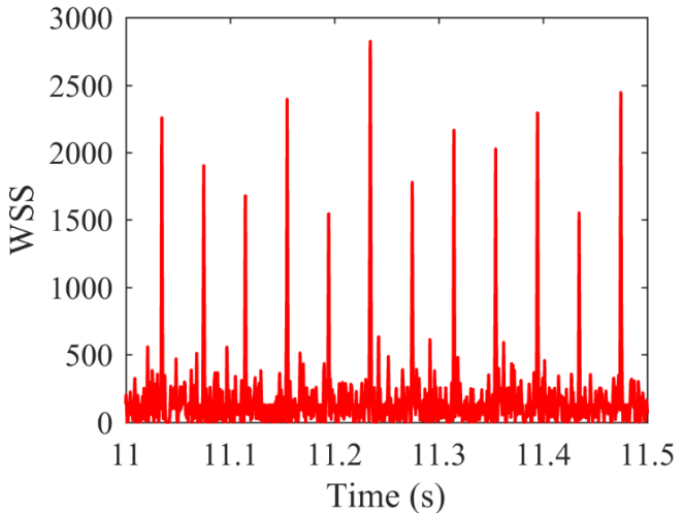

Fig. 27: SMR with a solution of 1 nM 40 nm Fluospheres, 1×TAE buffer, and 0.02% Tween-20. The reversal delay is 30 ms.

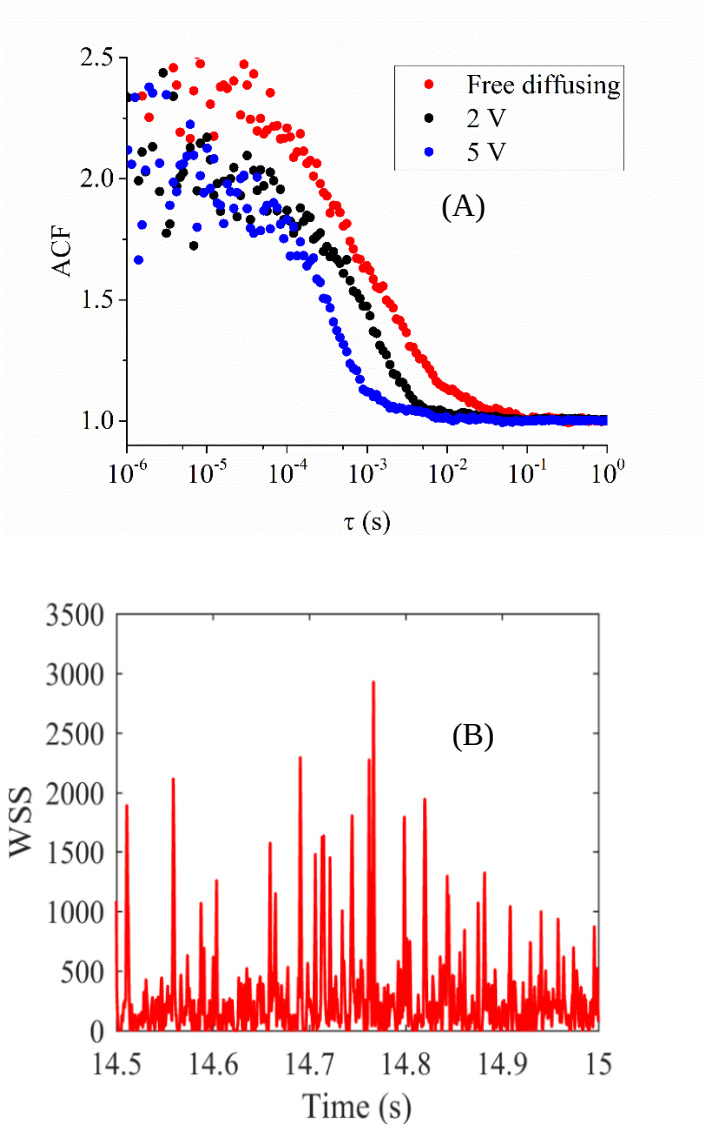

Fig. 28: (A) ACFs of dsDNA molecules driven by different voltages. (B) Result from an attempt at SMR using labeled dsDNA.

As seen in Fig. 29 A, the capillary has an inner diameter of 2 μm, an outer diameter of 150 μm, and is protected with a thin polyimide coating, which unfortunately gives a strong background fluorescence. To make the capillary microchannel, we first use a ceramic cleaving stone to chop the capillary into 1-inch pieces, then we remove the coating by baking for an hour at 700 °C. We then use silicone glue to fix the stripped capillary onto a glass coverslip and also to fix three o-rings above the capillary to the coverslip, as seen in Fig. 29 B. The two outer o-rings form reservoirs for the solution, and the o-ring in the middle is filled with the oil used for an immersion objective, which has the same refractive index as the coverslip (1.56). The oil has approximately the same refractive index as the fused silica capillary (1.46) and hence significantly reduces specular reflection and refraction at the cylindrical walls of the capillary.

To improve the capillary effect, we need to improve the hydrophilicity of the inner surface. We first rinse the capillary with 0.1 M sodium hydroxide (NaOH) for 5 minutes, then rinse with distilled water for 2 minutes, then rinse with running buffer, which is the same as that used in the nanochannels. After keeping the running buffer in the capillary for 10 minutes, we pipette in the working buffer containing 40 nm Fluospheres and start the experiment.

As shown in Fig 29 C, we are also able to use the piezo to recycle a Fluosphere that is freely diffusing in the capillary, but only for a short time before it diffuses beyond the 10 μm range of motion of the piezo. We are unable to perform SMR by electrokinetic flow, because the capillary is 10 mm long, much longer than the nanochannels (~0.1 mm), so the

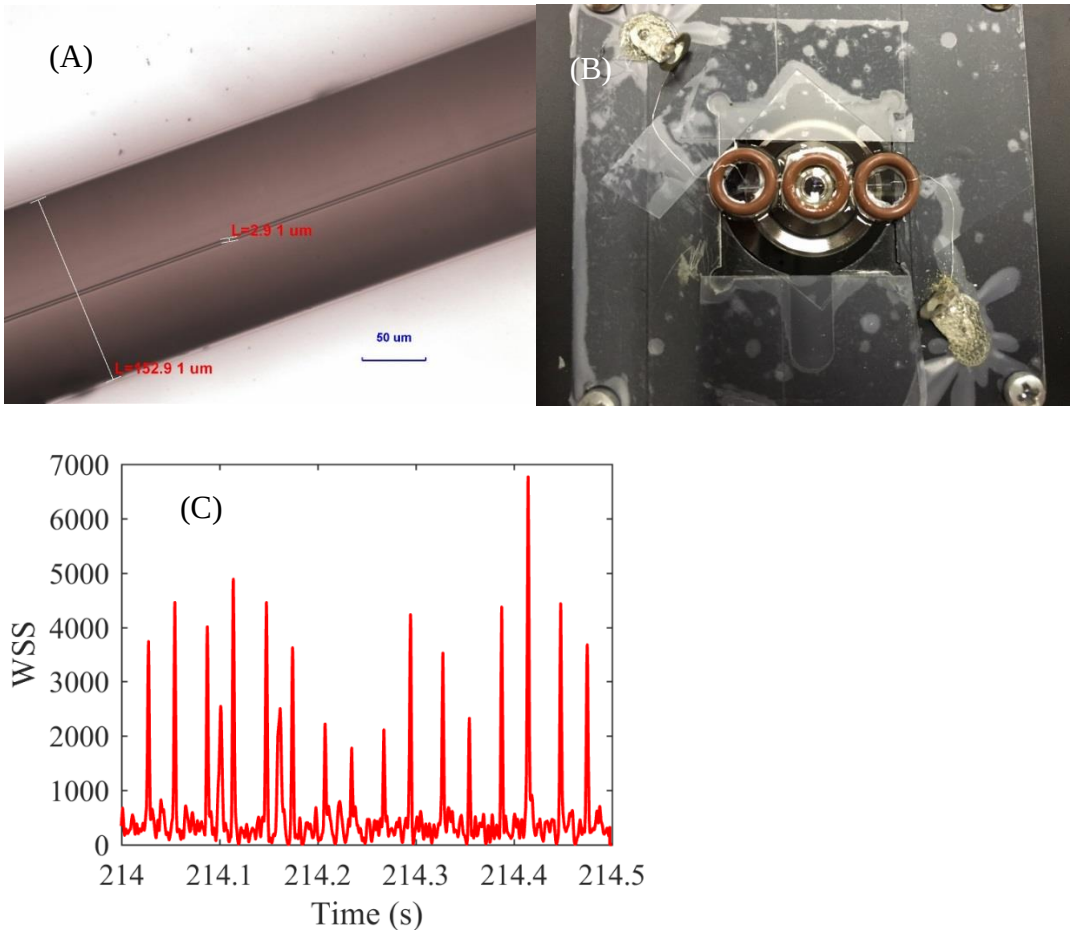

Fig. 29: (A) The size of the capillary tubing. (B) A finished capillary microchannel device. The o-rings on the sides are reservoirs of solution, and the o-ring in the middle is the observation window for the objective. This o-ring is filled with immersion oil to reduce refraction and reflection from the outer wall of the capillary. Two electrodes are connected to the reservoirs by platinum wires. (C) SMR using the piezo of a Fluosphere that appears to be freely diffusing along the capillary. The reversal delay is 30 ms.

electric field provided by the 20 V maximum potential difference output from the FPGA is inadequate to induce a flow in the capillary that is faster than the effective flow speed due to diffusion.

CHAPTER 6: EXPERIMENTAL RESULTS

This chapter presents details on the analysis of data from experiments. Section 6.1 discusses how to measure the beam waist and flow velocity from the autocorrelation of photon counts acquired from various experiments. Sections 6.2 and 6.3 discuss the measurement of single molecule diffusivities from SMR in capillary microchannels and nanochannels.

6.1 Measurement of beam waist and velocity

To measure the diffusivity of molecules using SMR, we need to know the beam waist ω_0 and the flow velocity v. The beam waist ω_0 can be experimentally measured by fitting the peak of the normalized autocorrelation function (ACF) [27] (ignoring the feature before ~1 μs, which is due to detector afterpulsing and triplet blinking), as illustrated in Fig. 30 A. The ACF of fluorescent particles within a 3-dimensionnal Gaussian-shaped probed-region was first proposed in Ref. [55]. In our experiment, the fluorescence photons are collected by SPADs and processed by a correlator program previously developed in our laboratory to calculate the normalized ACF.

If motion is restricted to one dimension, the fitting function with four fitting parameters a_0, a_1, a_2, and a_3, is

$$g(\tau) = a_0 + a_1 \exp\left(-a_2\tau^2/(1+a_3\tau)\right)\Big/\sqrt{1+a_3\tau}\,. \tag{6-1}$$

This functional form, which may be derived from first principles [56], is that expected for transport of a molecule in one dimension by diffusion and constant flow through a

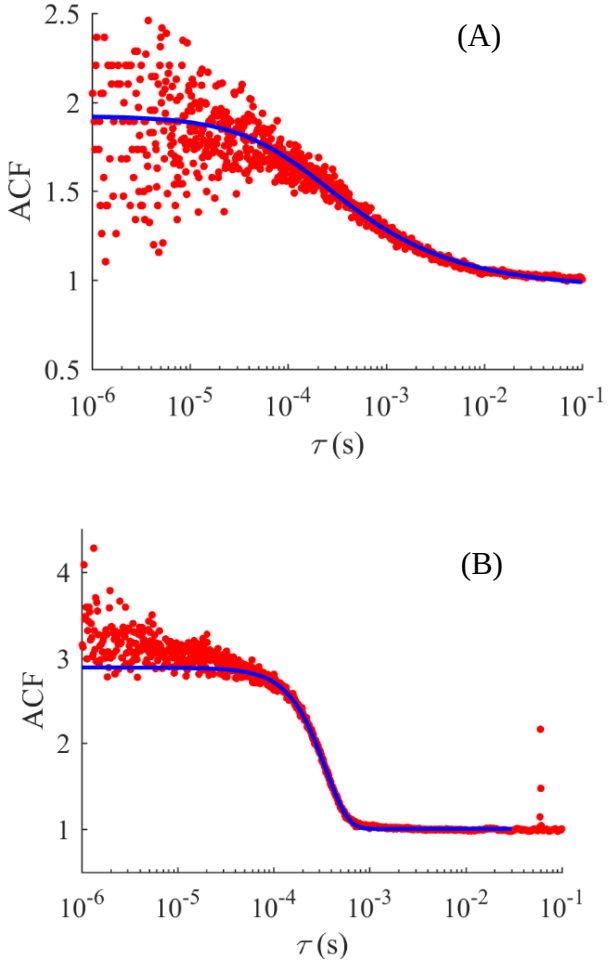

Fig. 30: (A) ACF of Alexa 647 conjugates free diffusing on a coverslip and fit to Eq. (5) of Ref. [27]. (B) ACF of Fluospheres recycling in a nanochannel and fit to Eq. (6-1).

Gaussian beam waist ω_0, where the molecule is confined by the nanochannel to move in only one dimension. In the case of molecules moving with constant velocity, $a_1 = F^2/(F+B)^2$, where F is the rate of fluorescence counts from a molecule at the center of the laser focus, and B is the background rate, and $a_0 = 1$, which gives $g(\infty) = 1$, as shown in Fig. 30 A. In the case of SMR, a_0 is the background level of the ACF between peaks, which may be less than 1, a_1 is the amplitude of the peak of the ACF, $a_2 = (v/\omega_0)^2$ is the square of the reciprocal of the time constant for flow, and $a_3 = 4D/\omega_0^2$ is the reciprocal of the time constant for diffusion.

We first measure ω_0 by recording fluorescence counts from freely diffusing Alexa 647 labeled streptavidin conjugates within a drop of solution on a coverslip, then fitting its ACF, as shown in Fig. 30 A. We divide a_3 by the diffusion coefficient, which is 1.3×10^{-10} m^2s^{-1} [57], and get ω_0 = 0.26 µm. Next, we measure *v* during SMR by applying a voltage across the nanochannel, performing SMR with Fluospheres, and again acquiring the ACF, as shown in Fig. 30 B. We fit the ACF to find a_2 and use the previously found value of ω_0 to derive *v*, which gives $v = 7.54 \times10^{-4}$ m/s. The location of the peak on the right of the slope in Fig. 30 B represents the 60 ms interval between two consecutive passages of Fluospheres. Also, we measure *v* during constant flow. Fig. 31 presents the fitting of the ACFs in Fig. 28 A, which gives $\omega_0/(2v)$ = 0.59 ms when the voltage is 2 V, and $\omega_0/(2v)$ = 0.18 ms when the voltage is 5 V. By substituting ω_0=0.26 µm we find the

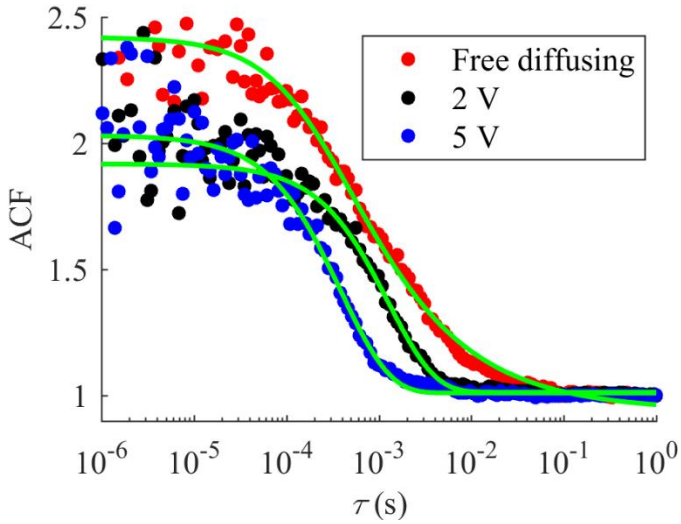

Fig. 31: Fit of the data in Fig. 28 (A) to Eq. (6-1).

flow speeds under 2 V and 5 V are 2.2×10^{-4} ms^{-1} and 7.2×10^{-4} ms^{-1} respectively.

As discussed in the last section of this chapter, in some experiments, we perform SMR in the capillary microchannel by using the piezo stage to move the capillary and molecule back and forth. To estimate the maximum translation speed attainable by the piezo stage, we move the piezo stage with a step-function command using the Nano-capture program, which is intended to be used to adjust the control parameters and test the response of the piezo stage. The measured maximum speed was 6.0×10^{-3} ms^{-1}. We then immobilize 40 nm Fluospheres on a glass coverslip with PDMS and fix the coverslip on the piezo stage. After positioning a Fluosphere into the center of the beam waist, we recycle the bead with our LabView program designed for SMR and calculate its ACF from the times of the detected photons. As seen in Fig. 32, the fit of the ACF gives $\omega_0/(2v) = 0.47$ ms. In this experiment, the laser beam is adjusted to fit the inner diameter of the capillary, which is 2 µm, hence the beam waist ω_0 is estimated to be 1 µm. This gives a translation speed of $v = 1.1 \times 10^{-3}$ ms^{-1}, which is smaller than the value measured by the Nano-capture software.

6.2 Results from single-molecule recycling in a capillary microchannel

For SMR in the capillary microchannel, an algorithm is developed to move the capillary with the molecule within it back and forth using the piezo stage, while adjusting the end points of the motion as the molecule diffuses along the capillary. To do so, the estimated position of the molecule is used as the center of the recycling and the piezo stage starts to move from a position that is a pre-scheduled distance dx (10,000 piezo units in the

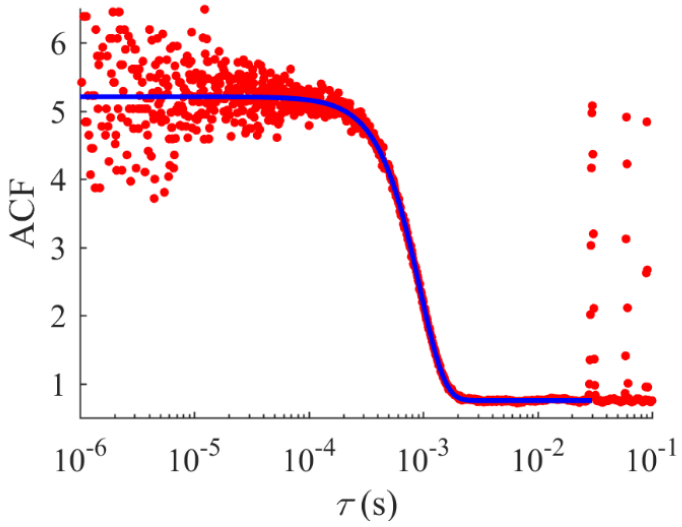

Fig. 32: ACF of immobilized Fluospheres in SMR using the laser beam for the capillary microchannel.

experiment, which is equal to 4.58 μm) away from the center. The piezo then remains at the destination for a certain period, which is equal to the reversal delay minus the time of translation. After this, the piezo is moved in the opposite direction and we use the estimated position of the molecule minus *dx* as the destination.

As the molecule diffuses in the microchannel, we must renew the estimated position of the molecule for each move. To estimate the current position of the molecule, we subtract the mean value of the distance between the time of the last WSS peak $t_w(i)$ and the starting time of the translation $t_p(i)$ from its current value and we multiply this by a scale factor *C*, which has dimensions of piezo units per millisecond. We then add the result to the previous center of the recycling to obtain a new estimated position for the molecule, as follows:

$$X(i+1) = \left[\left(t_w(i) - t_p(i)\right) - m\right] \times C + X(i)\,, \tag{6-2}$$

where $X(i)$ is the last estimated position of the molecule, $X(i + 1)$ is the estimated current position of the molecule, and *m* is the mean value of $X(i+1) - X(i)$. A measurement result obtained with the algorithm is illustrated in Fig. 33.

During the experiment, $X(i)$ and $t_p(i)$, as measured by the piezo clock as well as the FPGA clock, are all stored into one data file. From the collected data, the position of the molecule during the course of each translation can be derived using the following equation:

$$X_m(i) = X(i) - (-1)^i \left[\left(t_w(i) - t_p(i)\right)v - dx\right], \tag{6-3}$$

where *v* is the translation speed. Substituting $\Delta X(i) = \left(t_w(i) - t_p(i)\right)v$ into Eq. (6-3), we find the variation of position caused by diffusion is given by

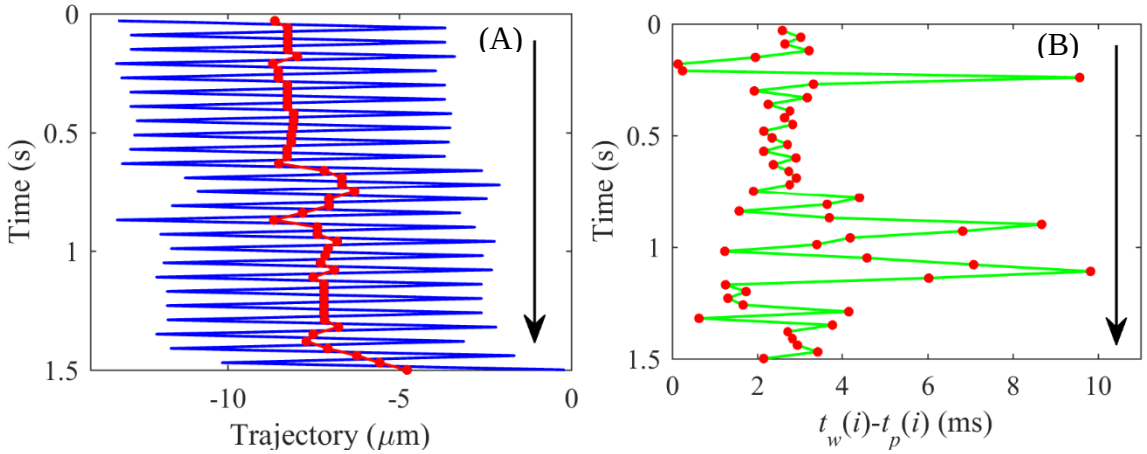

Wait until time = $t_p(i)$ (C)
If i is odd
piezo moves to $X(i) + dx$
else
piezo moves to $X(i) - dx$
Measure WSS peak at $t_w(i)$
calculate $X(i+1) = \left[\left(t_w(i) - t_p(i)\right) - m\right] \times C + X(i)$
Make $t_p(i+1) = t_p(i) + \Delta t$
Wait until time = $t_p(i + 1)$

Fig. 33 (A) Blue solid line is the trajectory of the piezo stage, the red dot is the center of the recycling. (B) The red dot is $t_w(i) - t_p(i)$ in each recycle. (C) The algorithm applied in the SMR with the piezo stage.

$$X_m(i+1) - X_m(i) = \left(X(i+1) - X(i)\right) + \left(-1\right)^i \left(\Delta X(ii+1) + \Delta X(ii) - 2dx\right). \quad (6\text{-}4)$$

Moreover, the diffusivity from a single measurement $\hat{D}_i$ is obtained from $\sqrt{2\hat{D}_i T} = X_m(i+1) - X_m(i)$, where T is the reversal delay. Substituting Eq. (6-4) gives

$$\hat{D}_i = \frac{1}{2T}\left[\left(X(i+1) - X(i)\right) + \left(-1\right)^i \left(\Delta X(ii+1) + \Delta X(ii) - 2dx\right)\right]^2. \quad (6\text{-}5)$$

The theory of ML gives $\hat{D} = \sum_i \hat{D}_i / N$, where N is the number of measurements. Thus

$$\hat{D} = \frac{1}{2TN}\sum_i \left[\left(X(i+1) - X(i)\right) + \left(-1\right)^i \left(\Delta X(ii+1) + \Delta X(ii) - 2dx\right)\right]^2. \quad (6\text{-}6)$$

To process the data files, we first reconstruct the WSS with the photon timings and record the peaks of bursts. Then we make a binned histogram of the times between the peaks and the starts in the FPGA clock and fit it with Gaussian functions, as shown in Fig. 34. As the piezo stage sometimes reaches its limit of motion and stops at the ends according to the algorithm, the molecule diffuses to the laser beam without the translation, which can cause the time between the peak and the start to be too short or too long. Therefore, we take the Gaussian function centered around 2.5 ms as the effective distribution and select the translations within a 3 sigma width of its peak. From Eq. (6-6), we can estimate the diffusivities of individual molecules. However, as SMR with the piezo stage is developed primarily to test our LabView program for SMR in the nanochannel, the estimated diffusivities can have large variations from the actual values. This is seen in Fig. 35, which presents the variation of the centers of recycles and the estimated diffusivities of individual Fluospheres from 4 datasets.

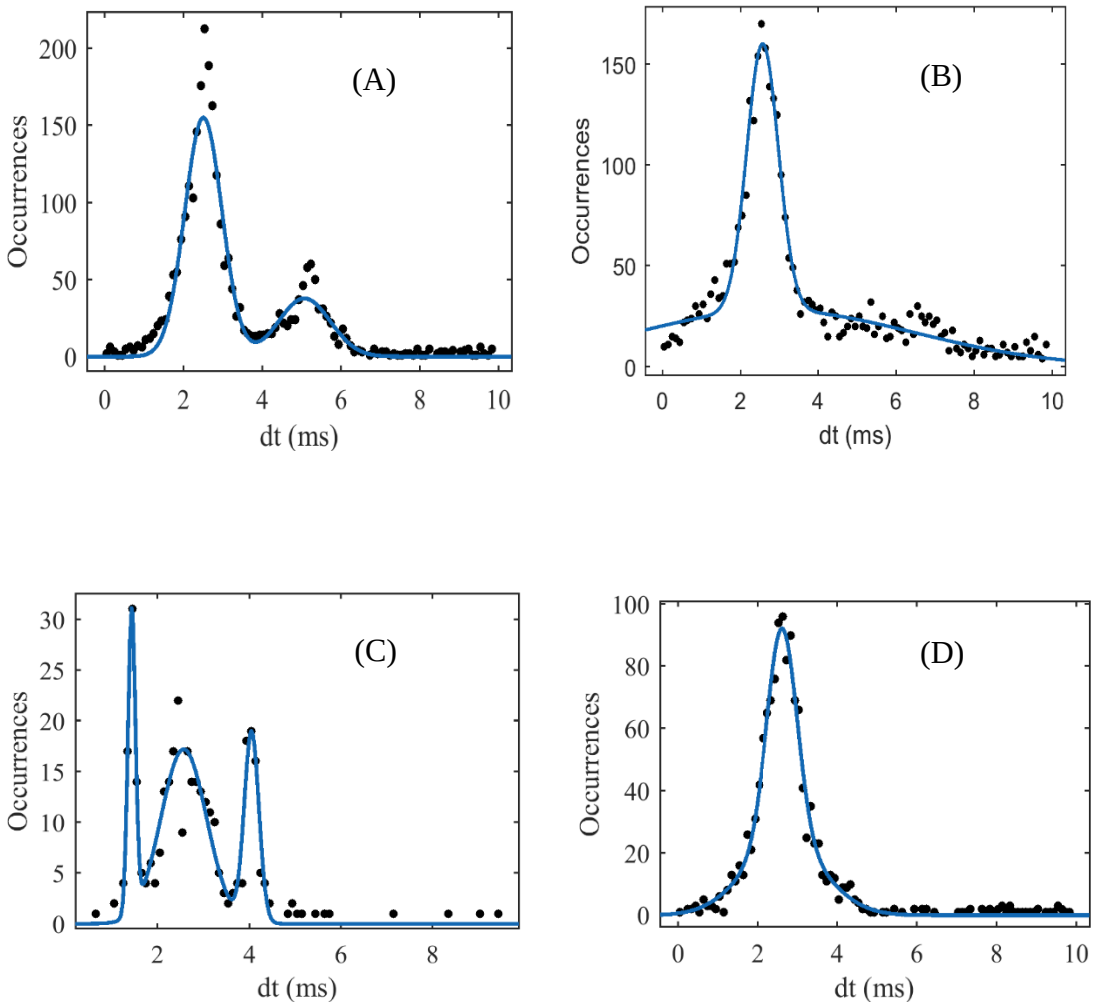

Fig. 34: Histograms of the gap between the peaks and the starts. The center of the effective distributions are (A) 2.516 ms, (B) 2.575 ms, (C) 2.575 ms, (D) 2.63 ms.

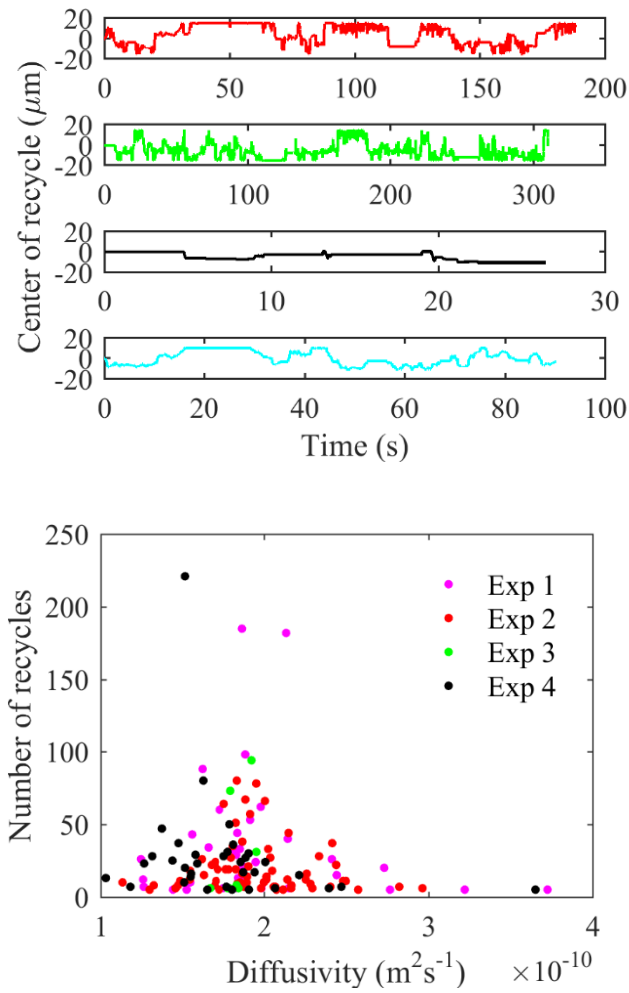

Fig. 35: Results from SMR in the capillary microschannel with the piezo stage. The upper graph shows the variations of centers of recyles. The bottom graph illustrates the estimated diffusivities of individual Fluospheres, which forms a Gaussian distribution centered around 1.8×10^{-10} m^2s^{-1}.

6.3 Results from single-molecule recycling in a nanochannel

As discussed in Chapter 5, we accomplished SMR in a nanochannel with Fluospheres. Because Fluospheres bleach very slowly, we can recycle them for thousands of times. Fig. 36 shows histograms of times between concecutive detections. The reversal delay in Fig. 36 A is 30 ms, and that in Fig. 36 B and C is 20 ms. The double peaks in Fig. 36 B indicate that a molecule takes a different time to move back versus forth in the nanochannel, which could be caused by a difference of electroosmosis in the two directions. To better process the data, we plot a finer binned histogram of Fig. 36 B and fit the double peak with two Gaussian functions.

Fig. 37 shows the fit of Fig. 36 B. After measuring the centers of the two Gaussian distributions, we categorize the times between consecutive detections into the two distributions and subtract the times of the corresponding centers, by which we can estimate the time variations caused by diffusion and hence calculate the diffusivity.

We estimate the diffusivities of individual Fluospheres by use of Eq. (2-16). Fig. 38 illustrates the result of the estimation, where Fluospheres from the 3 datasets are represented by different colors. The data in the graph shows that the diffusivity of Fluopheres in the nanochannel is of the magnitude of 10^{-13} m^2s^{-1}. Some Fluospheres are recycled for more than 1000 times, which illustrates that the recycling algorithm works. If the problem of surface adsorption can be solved, molecules such as DNAs and proteins could be studied with the system. Also, the algorithm could be improved to enable more recycles for a single molecule.

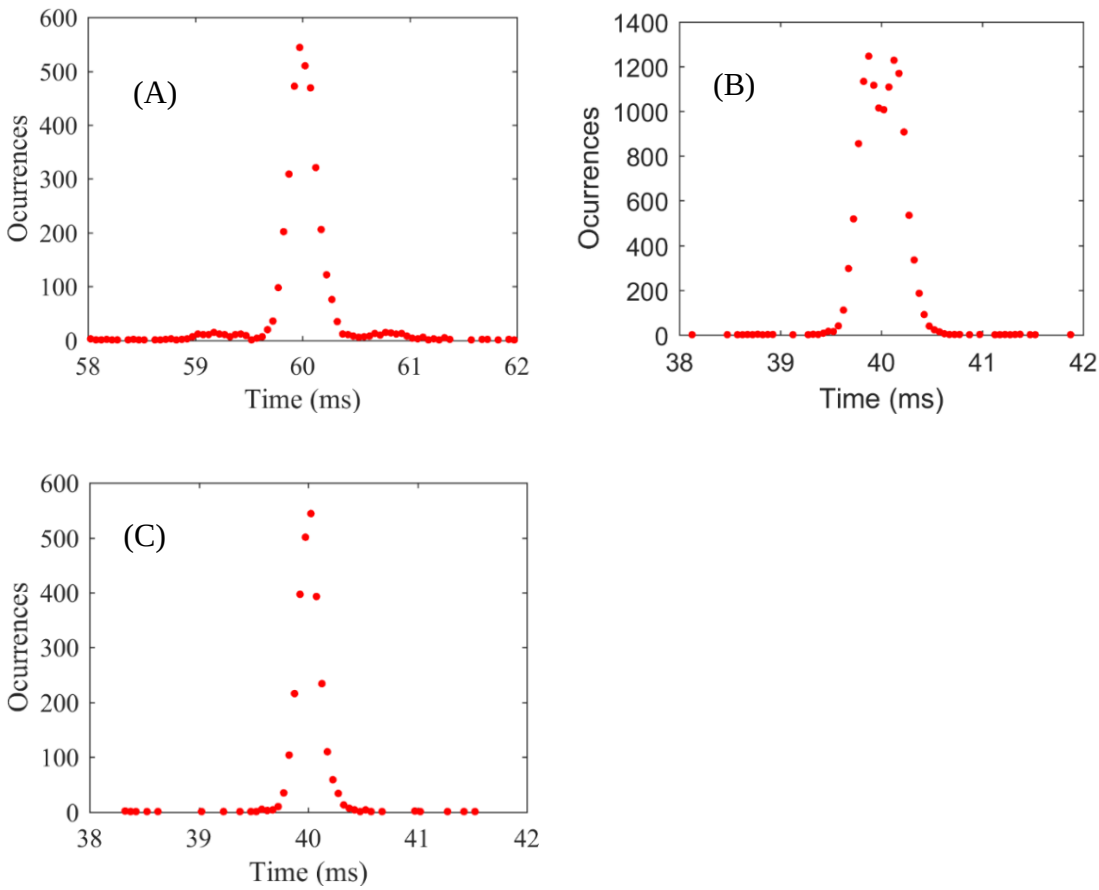

Fig. 36: The histograms of times between concecutive detections. (A) The center of the distribution is 60 ms. (B) Two distributions overlaps. The center of the left peak is 39.85 ms, and the center of the right peak is 40.14 ms. (C) The center of the distribution is 40 ms.

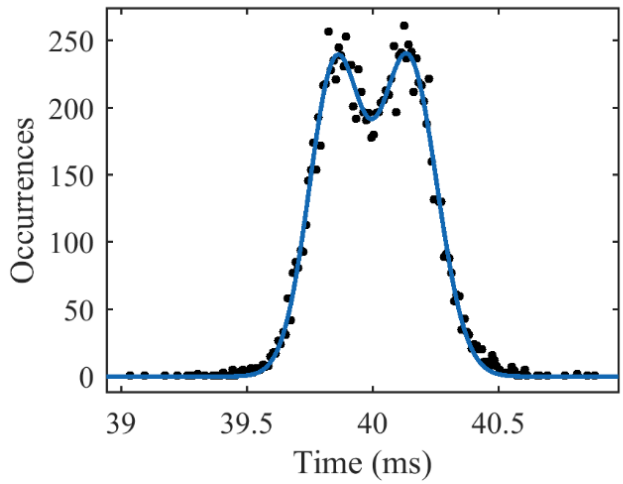

Fig. 37: The fitted histogram of Fig. 37 B.

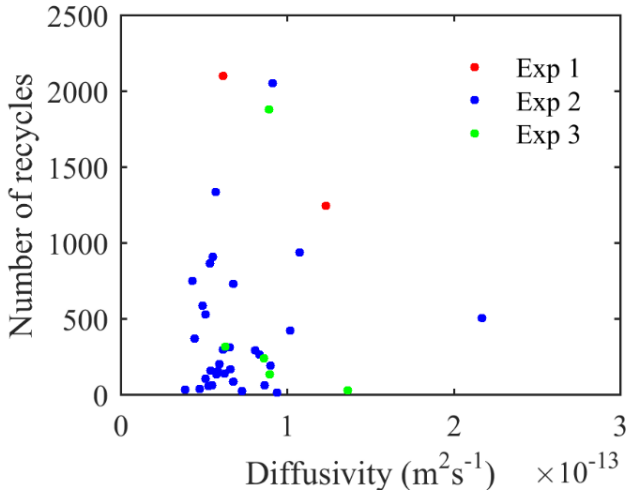

Fig. 38: The estimated diffusivities of 40 nm Fluospheres.

CHAPTER 7: SUMMARY AND FUTURE WORK

In this dissertation, single-molecule recycling is theoretically modeled using the Fokker-Planck equation, where the probability density function (pdf) of the molecule position disperses over time. Several methods for determining the time of passage of a molecule through the laser focus are compared. The weighted sliding sum method is more precise than the photon binning method. By averaging the times of detected photons within $\pm 3\sigma_t$ around the center of the WSS, the timing error of photon bursts obtained from the simulation is close to that of the theoretical prediction. The maximum-likelihood method is used to measure the diffusivities from the times of photon bursts. A lookup table is created to determine the evolution of the pdf of the diffusivity, and it is shown that two species, with diffusivities differing by a factor of 1.3, can in theory be resolved after about 200 recycles.

To investigate the feasibility of SMR of CdSe quantum dots, an Auger ionization model was developed to simulate the one-photon-excitation and two-photon-excitation of individual dots. The distribution of the "off" periods obtained from the simulation followed the "power law", which agreed with prior experimental results. The simulation indicated that a quantum dot could be recycled by using two-photon-excitation, but the number of recycles hardly reaches 200 times.

For experimental studies, a confocal microscope system is applied to single-molecule recycling in two systems: a capillary microchannel and a nanochannel. A NI PCI-7811R FPGA is programmed to apply weighted sliding sum calculations and to control the flow

or piezo motion direction during the recycling experiments. Capillary microchannels are fabricated to accomplish the preliminary experiments of single-molecule recycling and to test the feasibility of the control system. Nanochannels from a prior research project were reused, and various solution of molecules were applied to them. The result from recycling Fluospheres illustrates that the hardware of the system is capable of recycling a single molecule for more than one thousand times.

For future work, the non-specific adsorption to the surface could possibly be reduced by using improved buffer solution. Otherwise, the inner surface of the nanochannel could possibly be coated by a single-molecule layer to reduce its adherence to bio-molecules. Such attempts have been made by coating the inner surface of the nanochannel with PEG silane, but due to the congregation of the PEG silane molecules, the nanochannels were easily clogged. New nanochannels could be produced by electron beam lithography, and their diemnsions could be adjusted to improve the performance of SMR. The recycling algorithm could be upgraded to enable more recycles and eventually to recycle the majority of the molecules for more than 200 times. Simulation results show a molecule can be recycled for an average 205 times by use of an improved algorithm, which could be programmed into the LabView control system in the future.

LIST OF REFERENCES

1. Barkai, E., Jung, Y.J., and Silbey, R., *Theory of single-molecule spectroscopy: beyond the ensemble average.* Annual Review of Physical Chemistry, 2004. **55**: p. 457-507.
2. Moerner, W.E. and Fromm, D.P., *Methods of single-molecule fluorescence spectroscopy and microscopy.* Review of Scientific Instruments, 2003. **74**(8): p. 3597-3619.
3. Goldsmith, R.H. and Moerner, W.E., *Watching conformational- and photodynamics of single fluorescent proteins in solution.* Nature Chemistry, 2010. **2**(3): p. 179-186.
4. Rasnik, I., McKinney, S.A., and Ha, T., *Surfaces and Orientations: Much to FRET about?* Accounts of Chemical Research, 2005. **38**(7): p. 542-548.
5. Pang, Y.J. and Gordon, R., *Optical trapping of a single protein.* Nano Letters, 2012. **12**(1): p. 402-406.
6. Moerner, W.E., *New directions in single-molecule imaging and analysis.* Proceedings of the National Academy of Sciences of the United States of America, 2007. **104**(31): p. 12596-12602.
7. Enderlein, J., *Tracking of fluorescent molecules diffusing within membranes.* Applied Physics B: Lasers & Optics, 2000. **71**(5): p. 773.
8. Cohen, A.E., *Control of nanoparticles with arbitrary two-dimensional force fields.* Physical Review Letters, 2005. **94**(11): p. 118102.
9. Cohen, A., *Trapping and manipulating single molecules in solution.* Ph.D. Dissertation, Stanford University, 2006.
10. Cohen, A.E. and Moerner, W.E., *Controlling Brownian motion of single protein molecules and single fluorophores in aqueous buffer.* Optics Express, 2008. **16**(10): p. 6941-6956.
11. Davis, L.M., et al., *Electrokinetic delivery of single fluorescent biomolecules in fluidic nanochannels.* SPIE Proceedings, 2008. **7035**.
12. Davis, L.M., et al. *Feedback-driven microfluidic manipulation of a single fluorescent nanoparticle in solution as an alternative to optical trapping*. in *Optical Trapping Applications*. 2015. Optical Society of America.
13. King, J.K., Canfield, B.K., and Davis, L.M., *Three-dimensional anti-Brownian electrokinetic trapping of a single nanoparticle in solution.* Applied Physics Letters, 2013. **103**(4): p. 043102
14. Germann, J.A. and Davis, L.M., *Three-dimensional tracking of a single fluorescent nanoparticle using four-focus excitation in a confocal microscope.* Optics Express, 2014. **22**(5): p. 5641-5650.
15. Cang, H., et al., *Guiding a confocal microscope by single fluorescent nanoparticles.* Optics Letters, 2007. **32**(18): p. 2729-2731.
16. Wells, N.P., Lessard, G.A., and Werner, J.H., *Confocal, three-dimensional tracking of individual quantum dots in high-background environments.* Analytical Chemistry, 2008. **80**(24): p. 9830-9834.

17. Cohen, A.E. and Moerner, W.E., *Method for trapping and manipulating nanoscale objects in solution.* Applied Physics Letters, 2005. **86**(9): p. 093109.
18. Kayci, M. and Radenovic, A., *Single florescent nanodiamond in a three dimensional ABEL trap.* Scientific Reports, 2015. **5**: p. 16669.
19. Lesoine, J.F., et al., *Nanochannel-based single molecule recycling.* Nano Letters, 2012. **12**(6): p. 3273-3278.
20. Cipriany, B.R., et al., *Single Molecule Epigenetic Analysis in a Nanofluidic Channel.* Analytical Chemistry, 2010. **82**(6): p. 2480-2487.
21. Murphy, P.J., et al., *Single-molecule analysis of combinatorial epigenomic states in normal and tumor cells.* Proceedings of the National Academy of Sciences, 2013. **110**(19): p. 7772-7777.
22. Ghosh, S., et al. *Single-molecule fluorescence inside solid-state nanochannels*. in *Single Molecule Spectroscopy and Superresolution Imaging VII*. 2014. SPIE.
23. Robinson, W.N. and Davis, L.M., *Simulation of single-molecule trapping in a nanochannel.* Journal of Biomedical Optics, 2010. **15**(4): p. 045006
24. Shera, E.B., et al., *Detection of single fluorescent molecules.* Chemical Physics Letters, 1990. **174**(6): p. 553-557.
25. Bunfield, D.H. and Davis, L.M., *Monte Carlo simulation of a single-molecule detection experiment.* Applied optics, 1998. **37**(12): p. 2315-2326.
26. Nie, S.M., Chiu, D.T., and Zare, R.N., *Real-time detection of single-molecules in solution by confocal fluorescence microscopy.* Analytical Chemistry, 1995. **67**(17): p. 2849-2857.
27. Davis, L.M., et al., *Data reduction methods for application of fluorescence correlation spectroscopy to pharmaceutical drug discovery.* Current Pharmaceutical Biotechnology, 2003. **4**(6): p. 451-462.
28. Turin, G.L., *An introduction to matched-filters.* Ire Transactions on Information Theory, 1960. **6**(3): p. 311-329.
29. Weerakoon-Ratnayake, K.M., et al., *Electrophoretic separation of single particles using nanoscale thermoplastic columns.* Analytical Chemistry, 2016. **88**(7): p. 3569-3577.
30. Lyon, W.A. and Nie, S.M., *Confinement and detection of single molecules in submicrometer channels.* Analytical Chemistry, 1997. **69**(16): p. 3400-3405.
31. Pappaert, K., et al., *Measurements of diffusion coefficients in 1-D micro- and nanochannels using shear-driven flows.* Lab on a Chip, 2005. **5**(10): p. 1104-1110.
32. Magde, D., Elson, E., and Webb, W.W., *Thermodynamic fluctuations in a reacting system-measurement by fluorescence correlation spectroscopy.* Physical Review Letters, 1972. **29**(11): p. 705-708.
33. Krichevsky, O. and Bonnet, G., *Fluorescence correlation spectroscopy: The technique and its applications.* Reports on Progress in Physics, 2002. **65**(2): p. 251-297.

34. Dertinger, T., et al., *Two-focus fluorescence correlation spectroscopy: A new tool for accurate and absolute diffusion measurements.* Chemphyschem, 2007. **8**(3): p. 433-443.
35. Meseth, U., et al., *Resolution of fluorescence correlation measurements.* Biophysical Journal, 1999. **76**(3): p. 1619-1631.
36. Cohen, A.E. and Moerner, W.E., *Suppressing Brownian motion of individual biomolecules in solution.* Proceedings of the National Academy of Sciences of the United States of America, 2006. **103**(12): p. 4362-4365.
37. Michalet, X. and Berglund, A.J., *Optimal diffusion coefficient estimation in single-particle tracking.* Physical Review E, 2012. **85**(6): p. 14.
38. Vestergaard, C.L., *Optimizing experimental parameters for tracking of diffusing particles.* Physical Review E, 2016. **94**(2): p. 17.
39. Efros, A.L. and Rosen, M., *Random telegraph signal in the photoluminescence intensity of a single quantum dot.* Physical Review Letters, 1997. **78**(6): p. 1110-1113.
40. Dukes, A.D., et al., *Single-nanocrystal spectroscopy of white-light-emitting CdSe nanocrystals.* Journal of Physical Chemistry A, 2011. **115**(16): p. 4076-4081.
41. Papoulis, A., *Probability, random varuables, and stochastic processes*, ed. third. 1991.
42. Soper, S.A., et al., *The photophysical constant of several fluorescent dyes pertaining to ultrasensitive fluorescence spectroscopy.* Photochemistry and Photobiology, 1993. **57**(6): p. 972-977.
43. Pennycook, T.J., et al., *Dynamic fluctuations in ultrasmall nanocrystals induce white light emission.* Nano Letters, 2012. **12**(6): p. 3038-3042.
44. Nirmal, M., et al., *Fluorescence intermittency in single cadmium selenide nanocrystals.* Nature, 1996. **383**(6603): p. 802-804.
45. Kuno, M., et al., *Nonexponential "blinking" kinetics of single CdSe quantum dots: A universal power law behavior.* Journal of Chemical Physics, 2000. **112**(7): p. 3117-3120.
46. Kuno, M., et al., *"On"/"off" fluorescence intermittency of single semiconductor quantum dots.* Journal of Chemical Physics, 2001. **115**(2): p. 1028-1040.
47. Stefani, F.D., Hoogenboom, J.P., and Barkai, E., *Beyond quantum jumps: Blinking nanoscale light emitters.* Physics Today, 2009. **62**(2): p. 34-39.
48. Ye, M. and Searson, P.C., *Blinking in quantum dots: The origin of the grey state and power law statistics.* Physical Review B, 2011. **84**(12): p. 125317.
49. Messin, G., et al., *Bunching and antibunching in the fluorescence of semiconductor nanocrystals.* Optics Letters, 2001. **26**(23): p. 1891-1893.
50. van Oijen, A.M., et al., *Continuous-wave two-photon excitation of individual CdS nanocrystallites.* Applied Physics Letters, 2001. **79**(6): p. 830-832.
51. He, J., et al., *Observation of interband two-photon absorption saturation in CdS nanocrystals.* Journal of Physical Chemistry B, 2005. **109**(41): p. 19184-19187.

52. Wissert, M.D., et al., *Quantum dots as single-photon sources: Antibunching via two-photon excitation.* Physical Review B, 2011. **83**(11): p. 113304.
53. Gauderon, R., Lukins, P.B., and Sheppard, C.J.R., *Effect of a confocal pinhole in two-photon microscopy.* Microscopy Research and Technique, 1999. **47**(3): p. 210-214.
54. Denk, W., Strickler, J., and Webb, W., *Two-photon laser scanning fluorescence microscopy.* Science, 1990. **248**(4951): p. 73-76.
55. Elson, E.L. and Magde, D., *Fluorescence correlation spectroscopy .1. Conceptual basis and theory.* Biopolymers, 1974. **13**(1): p. 1-27.
56. Magde, D., Webb, W.W., and Elson, E.L., *Fluorescence correlation spectroscopy. 3. Uniform translation and laminar-flow.* Biopolymers, 1978. **17**(2): p. 361-376.
57. Zhang, L., et al., *Ligand–receptor binding on nanoparticle-stabilized liposome surfaces.* Soft Matter, 2007. **3**(5): p. 551-553.

APPENDIX

This MATLAB code is to generate the look-up table described by Eq. (2-26) from the ML estimated times of passages. By implementing this code, the evolution of the pdf of *D* and the estimated value of *D* can be obtained.

```
%read in the mat file of times of passages and number of misdetections
clear
clc
data=load('delay.mat','delay');
misdetect=data.delay(:,1); %number of misdetections
delay=data.delay(:,2); %time between two passages
new_molecule=data.delay(:,3); %if the molecule is newly loaded

%generate look up table
tw=1e-5; %time step for k
T=3e-2; %reversal delay
delta_t=1.5e-3; %time uncertainty
v=4.0e-4; %velocity of flow
e=(1:10000)'/10000; %e(j)
e_delta=e+(delta_t/T)^2;
d=(0:25000)'/3000; %d(k)
delay_k=round(abs(delay-2*misdetect.^2*T)./tw)+1;%delay in format of k
Dmax=v^2*T/4;
factor=misdetect.^2;%correction factor
%generate look-up table
s=@(k,t) -(log(factor(t)*e_delta)+d(k)^2./(factor(t)*e_delta))/2;

%estimate diffusivities
D=zeros(1000,2);%the measured diffusivities of individual molecules
S=zeros(10000,1);%the pdf of D
num_recycle=0;
jj=1;
for ii=1:size(delay,1)
    if new_molecule(ii)==0
            S=S+s(delay_k(ii),ii); %the pdf of D
            num_recycle=num_recycle+1;
    else %a new molecule is loaded, estimate the D of the previous one
        [s_max,j]=max(S); %measure D from the peak of the pdf
        D(jj,1)=e(j)*Dmax; %measured D
        D(jj,2)=num_recycle; %number of recycles
        S=s(delay_k(ii),ii);
        num_recycle=1;
        jj=jj+1;
    end
end
[s_max,j]=max(S);
D(jj,1)=e(j)*Dmax; %array of D
D(jj,2)=num_recycle; %array of number of recycles
D=D(1:jj,:);
```

VITA

Bo Wang was born in Jiamusi, Heilongjiang Province, China. He attended Jilin University in Changchun, China for his undergraduate study and graduated in 2010 with a Bachelor of Science degree in physics and a minor in Pharmaceutical Engineering. He then moved on to China Academy of Engineering Physics in Mianyang, China for graduate school and graduated in 2012 with a Master of Science degree in Optics. Bo continued his study at the University of Tennessee pursuing a Ph.D. degree in Physics with a minor in Computational Science since fall 2012.